



Numerical simulation of multiscale heat and moisture transfer in the thermal smart clothing system



Mao Aihua^{a,*}, Luo Jie^{b,*}, Li Guiqing^a, Li Yi^c

^a School of Computer Science & Engineering, South China University of Technology, Guangzhou, China

^b School of Fine Art and Artistic Design, Guangzhou University, Guangzhou, China

^c Institute of Textiles and Clothing, Hong Kong Polytechnic University, Hung Hom, Hong Kong

ARTICLE INFO

Article history:

Received 25 October 2013

Revised 21 April 2015

Accepted 20 October 2015

Available online 27 October 2015

Keywords:

Thermal smart clothing

Heat and mass transfer

Multiscale nonlinear models

Numerical simulation

ABSTRACT

Simulation capacity is essential to the engineering design of industrial products with complex functions. This paper discusses a numerical algorithm to simulate the multiscale heat and moisture transfer in the thermal smart clothing system. A group of multiscale nonlinear models are proposed to describe the mix-type coupled heat and moisture transfer in the human body, fabrics, fiber material, and phase change material (PCM) particles. The dynamic thermal boundary conditions among individuals are considered and described to integrate the multiscale models. The coupled partial differential equations of the models are discretized by the finite volume method, and the numerical scheme for the thermal smart clothing simulation are developed considering the specification of wearing scenarios. To validate the models and simulation scheme, the simulation results and experimental results with the same clothing and wearing conditions are compared and discussed. Furthermore, a series of simulation cases are made to present the application of this numerical algorithm in practical design by expressing a sequence of design issues through the simulation results for the designers. This simulation scheme is helpful in the engineering design process of thermal smart clothing to identify the thermal quality of the clothing in advance and thus reduce the design cost.

© 2015 Elsevier Inc. All rights reserved.

1. Introduction

Being regarded as an innovative product with great commercial prospect, thermal smart clothing is characterized by its capability to quantify the thermal performance of clothing to provide high-quality thermal protection for the human body under various wearing situations, such as extremely hot or cold environment. During the design process, the textile material is usually integrated with phase change material (PCM) particles or subjected to moisture management treatment or electrical heating technology. In contrast to traditional design, the engineering design method should be utilized. In this case the complex thermal and fluid flow among the human body, clothing, and the environment (called clothing wearing system) should be systematically considered to quantify the thermal quality of the clothing. However, these thermal and fluid flows are in different scales due to the different dimensions of the human body, fabric, fibers and PCM particles. It is difficult to have accurate analysis of the thermal performance of individual entity with numerical simulation only in one scale.

In the literature, interest is continuing on the mathematics of describing the heat and moisture transfer through porous textile materials. Theoretically, the involved heat transfer mechanisms include the conduction by the fibers and the intervening air,

* Corresponding authors. Tel.: +8602039380285.

E-mail addresses: ahmiao@scut.edu.cn (M. Aihua), jieluo@gzhu.edu.cn (L. Jie).

Nomenclature

B_{ij}	heat loss by blood flow in the j th body node in the i th segment (W)
C_a	water vapor concentration in the air filling the inter-fiber void space (kg/m ³)
C_f	water vapor concentration in the fiber (kg/m ³)
C_*	saturated water vapor concentration at the local temperature (kg/m ³)
c_v	volumetric heat capacity of the fabric (J/m ³ .K)
c_{ij}	thermal capacity of the j th body node in the i th segment (J/m ³ .K)
Ch_{ij}	heat production by muscle shivering of the j th body node in the i th segment (W/m ²)
D_a	diffusion coefficient of water vapor in the air of the fabric (m ² /s)
D_l	liquid diffusion coefficient in fabric (m ² /s)
D_f	diffusion coefficient of water vapor in the fiber (m ² /s)
D_{ij}	heat loss by radiation and convection of the j th body node in the i th segment (W/m ²)
E_{ij}	heat loss by evaporation of the j th body node in the i th segment (W/m ²)
F_R	thermal radiation flux on a tiny volume element to the left direction
F_L	thermal radiation flux on a tiny volume element to the right direction
G_a	coefficient of pressure gradient to water vapor flux
G_l	coefficient of pressure gradient to liquid water flux
G_s	coefficient of pressure gradient to air flux.
H_m	convection mass transfer coefficient (m/s)
H_c	convection heat transfer coefficient (W/m ² .K)
$m_{s,i}$	sweating secretion rate of the i th body segment (g/s.m ²)
$m_{rsw,i}$	regulatory sweating of the i th body node (g/s.m ²)
Γ_f	effective moisture sorption rate of the fiber
Φ_{lg}	evaporation/condensation rate of the liquid/vapor
L	thickness of the fabric (cm)
M_{ij}	metabolic heat of the j th body node in the i th segment (W/m ²)
Mb_{ij}	basal metabolic rate of the j th body node in the i th segment (W/m ²)
M_g	mole mass of air molecule (kg/mol)
h_{lg}	mass transfer coefficient for evaporation and condensation (m/s)
h_r	radiative heat transfer coefficient (W/m ² .K)
h_T	heat transfer coefficient between PCM particles and surrounding flow (W/m ² .K)
K_t	thermal conductivity of the fabric (W/m ² .K)
K_m	thermal conductivity of the PCM particle (W/m ² .K)
K_{ij}	thermal conductivity of the j th body node in the i th segment (W/m ² .K)
P_s	pressure of dry air in the fabric (Pa)
$P_{c,i}$	pressure of the clothing close to the skin of the i th body node (Pa)
$P_{sat,i}$	saturated vapor pressure of the skin of the i th body node (Pa)
$P_{sk,i}$	water vapor pressure of the skin of the i th body node (Pa)
P_e	pressure of the environment (Pa)
p_m	pumping ratio of water vapor loss from the skin
p_h	pumping ratio of heat loss from the skin
q_m	energy released/absorbed rate of PCM particle
R	general gas constant
R_{esk}	water vapor resistance of the skin (m ² .Pa.s/kg)
R_{va}	water vapor resistance of the air layer (m ² .Pa.s/kg)
R_{ta}	thermal resistance of the air layer (m ² K/W)
R_n	heat transfer resistance of waterproof membrane (m ² K/W)
RH_f	relative humidity of the fiber surface
r_f	fiber radius in radial coordinate (m)
r_m	PCM particle radius in radial coordinate (m)
S_i	area of the skin of the i th body node (m ²)
S_v	surface volume ratio of the fiber (1/m)
T	temperature of the fabric (K)
T_{ij}	temperature of the j th body node in the i th segment (K)
$T_{sk,i}$	skin temperature of the i th body node (K)
T_e	temperature of the environment (K)
$T_{c,i}$	temperature of the clothing close to the i th body node (K)

T_h	top temperature of self-heating wires (°C)
T_l	bottom temperature of self-heating wires (°C)
T_p	melting point of PCM particle (K)
t	time (s)
W	heat generation rate of the heating fabric (W/s)
WVP	water vapor permeability of the fabric (g/24h/cm ²)
W_f	weight of the fabric (g/m ²)
W_{ij}	heat production by external work on the j th body node in the i th segment (W/m ²)
W_n	moisture transfer resistance of waterproof membrane (s/m)
W_c	absorbed water content in the fiber
V_w	speed of walking (m/s)
V_e	speed of wind in the environment (m/s)

Greek symbols

ε_a	volume fraction of water vapor
ε_f	volume fraction of fibers
ε_l	volume fraction of liquid phase
ε_p	volume fraction of PCM particles
ε	porosity of the fabric
ρ_f	density of the fiber (kg/m ³)
ρ_m	density of PCM particle (kg/m ³)
τ_a	effective tortuosity of the fabric for water vapor diffusion
τ_l	effective tortuosity of the fabric for water liquid diffusion
β	radiation absorption constant of the fiber (1/m)
ω_a	proportion of the sorption of water vapor at fiber surface
ω_l	proportion of the sorption of liquid water at fiber surface
λ_v	latent heat of water vapor sorption or desorption by fibers (J/kg)
λ_l	latent heat of liquid water sorption or desorption by fibers (J/kg)
λ_{lg}	latent heat of evaporation of water (J/kg)
λ_m	latent heat of fusion of PCM particle (J/kg)
Σ	Stefan–Boltzmann constant (W/m ² .K)
η	dynamic viscosity of liquid water (Kg/m.s)

convection, and radiation. Meanwhile, the moisture in the vapor- and liquid-phase transfer mechanisms involves moisture diffusion, moisture absorption by the fibers, capillary effects, and moisture evaporation/condensation. The heat and moisture transfer process occurs when gradients in temperature and moisture concentration across the textile structures exist. Early research on this topic attempted to model these mechanisms using the laws of physics under steady-state condition [1–5]. The coupled heat and moisture transfer under transient condition in textile material was first described by Henry, further developed by Nordon and David, and improved by Li and Holcombe [6–8]. Several researchers incorporated the fiber moisture absorption model and considered the radiation heat flux in the coupled heat and moisture transfer through the fabric [9,10]. Zhu and co-workers improved the coupled model by considering the capillary liquid diffusion process in textiles [10,11]. Wang et al. considered the moisture evaporation/condensation process [12] to make the simulation results closer to the real situation. However, there are few research works which systematically investigated and simulated the thermal behaviors and interactions between the fibers, the fabrics, the functional treatments and coated materials.

Because the human body wears clothing most of the time, the thermal activities of the body usually interacts with the heat and moisture transfer in the clothing material. Some authors considered the human body as the boundary condition in the heat and mass transfer models of the fabric [13,14] or regarded clothing as the boundary condition for the human body bio-heat transfer [15–17]. Ghali [16] used a pair of coefficients to describe the heat and moisture transfer of the fabric. In these research investigations, either the human body or the clothing system is considered by simple process/coefficients or at a steady state. The spatially non-uniform and time-varying environments cannot be simulated with accurate results. Recent works also developed some algorithms on the simulation of heat and mass transfer through the fabric or garment, ignoring the thermal interaction between the clothing and the human body [18,19]. Thus, we must develop systematical and accurate models and numerical scheme to predict the variable thermal interaction between the human body and the clothing in response to the transient non-uniform environments.

In this paper, we consider the non-uniform thermal smart clothing wearing system and the dynamic interaction between the clothing and the human body. With regard to the multiscale dimensions of the human body, fabric, fiber material, and PCM particle, we propose a group of multiscale nonlinear models to describe accurately the mixed-type coupled heat and moisture flux in the individual entities. The boundary among the models with different scales is developed to integrate the effect of their interactions. The thermal functional treatments on the clothing, such as PCM coating, moisture management treatment,

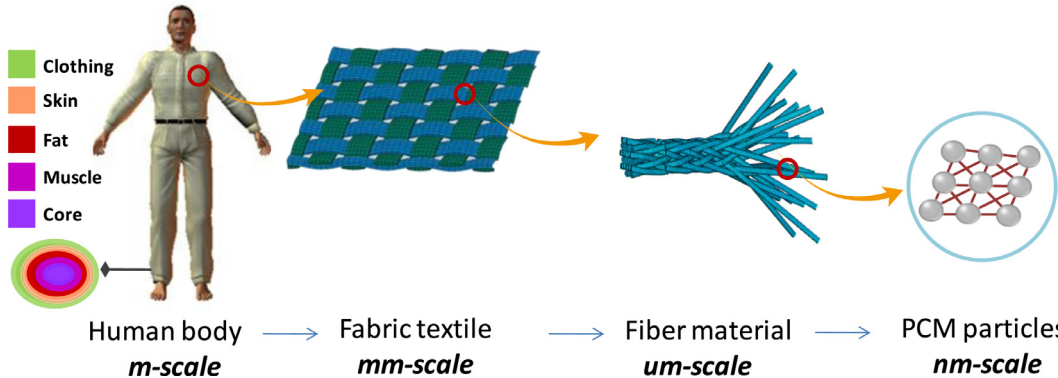


Fig. 1. Multiscale structure of the clothing wearing system.

waterproof membrane, and self-heating technology, are considered in the models. The finite volume method (FVM) is adopted to discretize the partial differential equations (PDEs) involved and the numerical solution is developed to implement the simulation. Comparison between the predicted and experimental results with the same clothing and wearing conditions is performed to validate the models and numerical solution. Finally, a series of simulation cases of utilizing the numerical algorithm in design application of thermal smart clothing is presented. The predicted results of the clothing and wearer are analyzed to help the designers in the engineering design process to confirm the issues before making the real prototypes.

2. Multiscale mathematical models

In theory, the transfer of heat and moisture in the clothing wearing system occurs in multiple phases and with a mixed type of coupling. The involved thermal-fluid processes include the followings:

- (i) Thermal bio-heat transfer of the human body in response to the external environment by blood vasodilatation or vasoconstriction, sweating, and muscle shivering;
- (ii) Simultaneous heat and moisture transfer across the fabric, which may be influenced by many factors such as phase change of the moisture, waterproof membrane, PCM, heat setting, and climatic conditions at the boundary;
- (iii) Moisture absorption/desorption in the fiber, which results in an increase in the heat flow or a decrease in the latent heat flow across the fabric;
- (iv) Absorption/release of the heat of PCM particles at their melting and crystallization points, which contributes to the delay of the change in temperature of the fabric exposed to a very hot/cold environment.

The thermal processes involved above are in different scales due to the different dimensions of the entities. Namely, the heat storage process of the PCM particles is in the nanometer scale; the fiber moisture sorption/desorption is in the micrometer scale; the fabric heat and moisture transfer process is in the millimeter scale; and the thermal regulation of the human body is in the meter scale. A representative illustration of the multiscale clothing wearing system is shown in Fig. 1, which shows that the difference among the scales is 1000 times. Full-field modeling and simulation of these multiscale thermal-fluid processes are important to achieve more accurate prediction on the complex thermal smart clothing system.

The multiscale mathematical models proposed for the thermal smart clothing wearing system are based on the following assumptions:

- (i) The human body consists of six segments, including the head, trunk, arm, leg, hand, and foot; each segment is composed of four concentric layers of core, muscle, fat, and skin.
- (ii) The fabric is porous and isotropic consisting of fibers and inter-fiber void space, and may be treated with PCM coating, moisture management treatment, waterproof membrane and self-heating wires.
- (iii) Local thermal equilibrium exists among all phases because of the small dimension of the pores in the fabric; thus, all phases have identical temperature at a point in space.
- (iv) The inertial force of each phase in the porous fabric is negligible.
- (v) Volume swelling of the fibers due to the change in the moisture content is neglected, and the moisture content at the fiber surface is in equilibrium with that of the surrounding air.
- (vi) The radii of the PCM particles are identical and uniformly embedded in the fabric.

2.1. Bio-heat transfer model in the meter scale

In the bio-heat transfer process of the human body, subsequent to the analytical bio-heat models [20,21], the multi-node single-segment models and multi-segment models of the human body are the most representative ones, such as the Gagge's

two-node single-segment model [22] and Stolwijk's 25-node multi-segment model [23]. The multi-node models have many applications and been widely validated by thousands of experiments due to their computational simplicity but high effectiveness. For instance, Ghaddar et al. [24] used a modified Gagge's two-node model to simulate the human physiological responses for prediction of the clothing insulation under periodic ventilation, further they [25] extended it into a two-node multi-segment model for integration with clothing ventilation models to predict segmental response of humans needed for assessing local and overall comfort. The multi-segment bio-heat models regard the human body as multiple segments and each one consists of a set of layers for modeling the bio-heat process, and thus has better precision and flexibility than the previous ones [26]. For instance, Salloum et al. [27] improved the Stolwijk's model with 15 cylindrical segments while Tanabe et al. [28] extended into a 16 body segments and 65-node thermoregulation model. More typically, the UC Berkeley comfort model is also originated from the Stolwijk's model, which can theoretically simulate unlimited body segments for predicting human physiological response to transient, non-uniform thermal environments [29]. Fiala et al. proposed a multi-segmental model consisting of controlled passive system and controlling active system to describe the dynamic heat transport within the body and exchanged with the environment [30]. In the previous work, [24,25] used a 1D linear three node to model the heat and moisture transport through the fabric, [28,30] used parameters to express the clothing insulation and area for individual segment, [27] assimilated the fabric layer as a cylinder neglecting the effect of moisture in the fabric and assuming evaporative and dry resistances of the fabrics as constant, and [29] added a clothing node to model both heat and moisture capacitance of clothing. It can see they simplified or neglected the complex heat and moisture processes within the clothing and the interaction between the human body and clothing for the purpose of computation efficiency.

In this paper, we model the complex heat and moisture transfer in the different scales of the thermal smart clothing system to have precise prediction results of the performance of thermal smart clothing. The overall computation loads are dependent on the clothing models and also on the integration dimensions with the human bio-heat transfer models. In order to balance the computation accuracy and efficiency, the Stolwijk's 25-node model [23] is adopted and improved to model the bio-heat transfer of the human body and interact with the clothing models on 6 body segments. That is, the human body is divided into six segments with four layers in each segment. All the layers in the segments are regarded as individual nodes, which are connected by an additional central blood node representing the blood circulation of the whole body. Within each segment, heat is transferred through the layers via conduction. The blood node exchanges heat with all other nodes via convection. Let i denote the body segments ($1 = \text{head}$, $2 = \text{trunk}$, $3 = \text{arm}$, $4 = \text{hand}$, $5 = \text{leg}$, $6 = \text{foot}$) and j denotes the layer in each segment ($1 = \text{core}$, $2 = \text{muscle}$, $3 = \text{fat}$, $4 = \text{skin}$), the heat balance equations for each body node are expressed as follows [23]:

For the core, muscle, fat and skin nodes:

$$c_{i,j} \frac{dT_{i,j}}{dt} = M_{i,j} - B_{i,j} - K_{i,j} - D_{i,j} - E_{i,j} \quad (i = 1, 2, \dots, 6, j = 1, 2, \dots, 4), \quad (1)$$

where the left side of the equation is the accumulated heat in the body node, $c_{i,j}$, and $T_{i,j}$ are the thermal capacity and the temperature of each node respectively; on the right side, $M_{i,j}$, $B_{i,j}$, $K_{i,j}$, $D_{i,j}$ and $E_{i,j}$ are the metabolic heat, heat loss by blood flow, thermal conductive heat, heat loss by radiation and convection and heat loss by evaporation of each node respectively.

For the blood node:

$$c_b \frac{dT_b}{dt} = \sum_{i=1}^6 \sum_{j=1}^4 B_{i,j}, \quad (2)$$

where the left side of the equation is the accumulated heat in the blood node, the right side is the sum of the blood flow heat by all nodes in the 6 segments.

The metabolic heat of the body ($M_{i,j}$) is calculated by:

$$M_{i,j} = Mb_{i,j} + W_{i,j} + Ch_{i,j}, \quad (3)$$

where the $Mb_{i,j}$ is the basal metabolic rate of each node, $W_{i,j}$ is the heat production by external work of each node, $Ch_{i,j}$ is the heat production by muscle shivering of each node.

Considering the interactions between the skin and the clothing, their boundary can be described through the heat and mass flux [31]. To calculate the evaporative heat loss ($E_{i,j}$) from the skin, we must model the sweat accumulation on the skin surface [32].

For the skin layer ($j = 4$) of each body segment, we have

$$D_{i,4} = \underbrace{H_c(T_{i,4} - T_{c,i})}_{\text{convective heat transfer between the skin and clothing}}, \quad (4)$$

$$E_{i,4} = \underbrace{H_m \lambda_{lg}(P_{sk,i} - P_{c,i})}_{\text{latent evaporation heat between the skin and clothing}}, \quad (5)$$

$$\frac{dm_{s,i}}{dt} = m_{rsw,i} + \underbrace{\frac{P_{sat,i}(T_{sk,i}) - P_{sk,i}}{R_{esk}}}_{\text{perspiration}} - \underbrace{\frac{H_m(P_{sk,i} - P_{c,i})}{R_{esk}}}_{\text{evaporation from skin to clothing}}, \quad (6)$$

where $m_{s,i}$ is sweating secretion rate of each body segment, $P_{sat,i}(T_{sk,i})$ denotes the saturated vapor pressure at temperature ($T_{sk,i}$)

When no sweat accumulates on the skin surface, the water vapor pressure of the skin ($P_{sk,i}$) is determined by the moisture equilibrium of skin sweating:

$$P_{sk,i} = \frac{m_{rsw,i}R_{esk} + P_{sat,i}(T_{sk,i}) + P_{c,i}R_{esk}H_m}{H_mR_{esk} + 1}, \quad (7)$$

Otherwise it will be the saturated vapor pressure:

$$P_{sk,i} = P_{sat,i}(T_{sk,i}). \quad (8)$$

Remark 1. To describe the dynamic interactions at the boundary, the values of the temperature of inner clothing ($T_{c,i}$) and the pressure of inner clothing ($P_{c,i}$) should be the predicted temperature and pressure of the inner fabric of the clothing at the same time point with skin temperature ($T_{sk,i}$).

For the body segment without clothing, we have

$$D_{i,j} = \underbrace{\frac{T_{i,4} - T_e}{R_{ta}}}_{\text{direct heat transfer from skin to air}}, \quad (9)$$

$$E_{i,j} = \underbrace{\frac{S_i(P_{sk,i} - P_e)}{R_{va}}}_{\text{latent evaporation heat from skin to air}}, \quad (10)$$

$$\frac{dm_{s,i}}{dt} = m_{rsw,i} + \underbrace{\frac{P_{sat,i}(T_{sk,i}) - P_{sk,i}}{R_{esk}}}_{\text{perspiration}} - \underbrace{\frac{(P_{sk,i} - P_e)}{R_{va}}}_{\text{evaporation from skin to air}}. \quad (11)$$

When there is no sweat accumulated on the skin surface, Eq. (7) becomes

$$P_{sk,i} = \frac{m_{rsw,i}R_{esk}R_{va} + P_{sat,i}(T_{sk,i})R_{va} + P_eR_{esk}}{R_{esk} + R_{va}}. \quad (12)$$

According to [15], the thermal resistance of the air layer (R_{ta}) and the water vapor resistance of the air layer (R_{va}) are calculated by:

$$R_{ta} = \frac{1}{h_r + 8.3 \times \sqrt{0.11 + 0.45V_w + V_e}}, \quad (13)$$

$$R_{va} = \frac{1}{0.1353 \times \sqrt{0.11 + 0.45V_w + V_e}} \times 2430 \times 1000. \quad (14)$$

Remark 2. V_w and V_e are the control variables by which we can simulate the wearing scenarios with different walking speeds of the human body and the wind speeds of the environment.

2.2. Coupled heat and moisture transfer model in the millimeter scale

Garment is usually constructed with one or multiple fabrics, which, in general, have millimeter-scale thickness. Because the heat and moisture transfer flux in the fabric mostly exists across the thickness direction [33], the heat and moisture balance equations are given in terms of the thickness dimension. Because of the accompanying phase change phenomena caused by PCM, moisture absorption/desorption by the fiber, or moisture condensation/evaporation, the heat and moisture transfer process during the transient process are dynamically coupled. Meanwhile, we also consider the pressure effect on the heat and moisture transfer.

Let x denote the coordinate across the thickness of the fabric, $x = 0$, and $x = L$ respectively indicate positions at the inner and the outer surfaces of the fabric, and t denotes the time. According to [6, 33–35], the governing equations for the coupled heat and moisture transfer process across the fabric can be modeled as

$$\underbrace{\varepsilon_a \frac{\partial C_a}{\partial t} - C_a \frac{\partial \varepsilon_l}{\partial t}}_{(1t)} = \underbrace{\frac{\varepsilon_a D_a}{\tau_a} \frac{\partial^2 C_a}{\partial x^2}}_{(2t)} + \underbrace{G_a \frac{\partial^2 P_s}{\partial x^2}}_{(3t)} + \underbrace{\sum \varpi_a \varepsilon_f \Gamma_f}_{(4t)} + \underbrace{\Phi_{lg}}_{(5t)}, \quad (15)$$

$$\rho_l \frac{\partial \varepsilon_l}{\partial t} = \underbrace{\rho_l \frac{\partial}{\partial x} \left(D_l \frac{\partial \varepsilon_l}{\partial x} \right)}_{(6t)} + \underbrace{G_l \frac{\partial^2 P_s}{\partial x^2}}_{(7t)} + \underbrace{\sum \varpi_l \varepsilon_f \Gamma_f}_{(8t)} - \underbrace{\Phi_{lg}}_{(9t)}, \quad (16)$$

$$c_v \frac{\partial T}{\partial t} = \underbrace{\frac{\partial}{\partial x} \left(K_t \frac{\partial T}{\partial x} \right)}_{(10t)} + \underbrace{\frac{\partial F_R}{\partial x} - \frac{\partial F_L}{\partial x}}_{(11t)} + \underbrace{\sum (\varpi_a \lambda_v + \varpi_l \lambda_l) \varepsilon_f \Gamma_f}_{(12t)} - \underbrace{\lambda_{lg} h_{lg} \Phi_{lg}}_{(13t)} + \underbrace{\varepsilon_p q_m}_{(14t)} + \underbrace{W}_{(15t)}, \quad (17)$$

$$\underbrace{\frac{M_g \varepsilon_a}{RT} \frac{\partial P_s}{\partial t} - \frac{P_s \varepsilon_a M_g}{RT^2} \frac{\partial T}{\partial t} - \frac{M_g P_s}{RT} \frac{\partial \varepsilon_l}{\partial t}}_{(16t)} = \underbrace{\frac{\partial}{\partial x} \left[G_s \frac{\partial P_s}{\partial x} \right]}_{(17t)} - \underbrace{\varpi_a \varepsilon_f \frac{\partial C_f}{\partial t} + \Phi_{lg}}_{(18t)}. \quad (18)$$

Eq. (15) is the water vapor balance equation, in which the left side is accumulated water vapor in the fabric (1t), the right side include the water vapor by diffusion (2t), the water vapor by pressure gradient (3t), the water vapor by all composed fibers' moisture absorption/desorption (4t) and the water vapor by moisture evaporation/condensation (5t).

Eq. (16) is the liquid water balance equation, the left side is accumulated liquid water in the fabric, the right side include the liquid volume by diffusion (6t), the liquid volume by pressure gradient (7t), the liquid volume by all composed fibers' moisture absorption/desorption (8t) and the liquid volume by moisture evaporation/condensation (9t).

Eq. (17) is the energy balance equation, in which the left side is the accumulated heat in the fabric, the right side include the conductive heat in the fabric (10t), the heat by radiation in the fabric (11t), the heat released by all composed fibers' moisture evaporation/condensation (12t), the heat released by moisture evaporation/condensation(13t), the heat released by PCM particles (14t) and the heat produced by self-heating wires (15t).

Eq. (18) is the gas (water vapor and air) balance equation, in which the left side is the summed accumulated gas in the fabric (16t), the right side include the air flux by pressure (17t) and the water vapor by fiber moisture absorption/desorption and moisture evaporation/condensation (18t).

Considering that the liquid water diffuses across the fabric mainly through capillary effects, the diffusion coefficient (D_l) is calculated by the capillary pore distribution (d_c), fiber surface energy (γ), effective angle of the capillaries (α), contact angle (θ), liquid volumetric fraction (ε_l), and dynamic viscosity (μ_l) and porosity (ε) of the fabric [33]:

$$D_l = \frac{3\gamma \cos \theta \sin^2 \alpha d_c \varepsilon_l}{20\mu_l \varepsilon}. \quad (19)$$

Remark 3. The variables of contact angle (θ), effective angle of the capillaries (α) and effective tortuosity of water liquid diffusion (τ_l) are the means to control the effect of moisture management on the fabric [36].

Moisture evaporation/condensation happens when a difference between the current and the saturated moisture concentration exists, which can be calculated:

$$\Phi_{lg} = \frac{\varepsilon_a}{\varepsilon} h_{lg} S_v (C^*(T) - C_a). \quad (20)$$

In Eqs. (15)–(18), the coefficient of pressure gradient to water vapor flux (G_a), coefficient of pressure gradient to liquid water flux (G_l), and coefficient of pressure gradient to air flux (G_s) are calculated by the following equations [34]:

$$G_a = C_a \frac{3\varepsilon \sin^2 \alpha d_c^2}{80\mu_a} \left(1 - \left(\frac{\varepsilon_l}{\varepsilon} \right)^3 \right), \quad (21)$$

$$G_l = \rho_l \frac{3\varepsilon \sin^2 \alpha d_c^2}{80\mu_l} \left(\frac{\varepsilon_l}{\varepsilon} \right)^3, \quad (22)$$

$$G_s = \frac{M_g P_s}{RT} \frac{3\varepsilon \sin^2 \alpha d_c^2}{80\mu_s} \left(1 - \left(\frac{\varepsilon_l}{\varepsilon} \right)^3 \right). \quad (23)$$

The boundary condition equations are developed according to the possible position of the fabric in the clothing wearing system, namely:

(i) The fabric position is next to the skin

The heat and moisture flux from the body skin exerts its effect at the boundary. The boundary condition equations are

$$\left. \frac{D_a \varepsilon_a}{\tau_a} \frac{\partial C_a}{\partial x} \right|_{x=0} = \underbrace{-\frac{\varepsilon_a}{\varepsilon} H_m (C_{sk,i} - C_a)}_{\text{convective water vapor from skin to fabric}} - \underbrace{\frac{p_m}{\lambda} E_{sk,i}}_{\text{water vapor from sweat}}, \quad (24)$$

$$\left. \frac{D_l \rho_l}{\tau_l} \frac{\partial \varepsilon_l}{\partial x} \right|_{x=0} = \underbrace{\frac{\varepsilon_l}{\varepsilon} h_{lg} (C^*(T) - C_a)}_{\text{liquid water by condensation in boundary}}, \quad (25)$$

$$\left. K_t \frac{dT}{dx} \right|_{x=0} = \underbrace{-(1-p_h) H_c (T_{sk,i} - T)}_{\text{convective heat from skin to fabric}} - \underbrace{\lambda_{lg} h_{lg} (C_{sk,i} - C^*(T))}_{\text{heat by condensation in boundary}}, \quad (26)$$

$$P_{s,0} = P_{sk,i}. \quad (27)$$

Remark 4. In Eq. (26), p_m and p_h are the pump ratios of the water vapor and the heat loss from the skin respectively, which are determined by the fitting design of the garment, such as loose-fit, just-fit, and tight-fit.

(ii) The fabric position is next to the environment

The heat and moisture flux directly flows to the environment. The boundary condition equations are

$$\frac{D_a \varepsilon_a}{\tau_a} \frac{\partial C_a}{\partial x} \Big|_{x=L} = \underbrace{\frac{\varepsilon_a}{\varepsilon} H_m (C_e - C_a)}_{\text{convective heat from fabric to environment}}, \quad (28)$$

$$\frac{D_l \rho_l}{\tau_l} \frac{\partial \varepsilon_l}{\partial x} \Big|_{x=L} = \underbrace{\frac{\varepsilon_l}{\varepsilon} h_{lg} (C_a - C * (T_e))}_{\text{liquid water by condensation in boundary}}, \quad (29)$$

$$K_t \frac{dT}{dx} \Big|_{x=L} = \underbrace{H_c (T_e - T)}_{\text{convective heat from fabric to environment}} + \underbrace{\frac{\varepsilon_l}{\varepsilon} \lambda_{lg} h_{lg} (C_e - C^*(T))}_{\text{heat by condensation in boundary}}, \quad (30)$$

$$P_{s,L} = P_e. \quad (31)$$

Remark 5. The effect of a waterproof membrane on the heat and moisture transfer in the fabric is considered through the convective water vapor transfer coefficient (H_m) and the connective heat transfer coefficient (H_c) [37].

Thus, the combined effective coefficients become

$$\bar{H}_m = \frac{1}{W_n + \frac{1}{H_m}}, \quad (32)$$

$$\bar{H}_c = \frac{1}{R_n + \frac{1}{H_c}}. \quad (33)$$

2.3. Moisture absorption/desorption model in the micrometer scale

In the fabric, the moisture exchange between the fibers and adjacent air crosses the fiber radius, which is generally in the micrometer scale. When moisture is present in the void space, the fiber will continuously absorb the moisture until its moisture content is saturated; on the other hand, it may desorb additional moisture to attain equilibrium with the surrounding air. Considering this two-stage process [35], a uniform equation can be described in radial coordinates:

$$\frac{\partial C_f}{\partial t} = \frac{1}{r_f} \frac{\partial}{\partial r_f} \left(r_f D_f \frac{\partial C_f}{\partial r_f} \right), \quad (34)$$

where C_f is the water vapor concentration in the fiber and r_f is the fiber radius in radial coordinate.

At the boundary between the fiber surface and the adjacent air, the amount of absorbed/desorbed moisture depends on the air relative humidity; thus

$$C_f|_{r=0} = \rho_f W_c (RH_f), \quad (35)$$

where W_c is the absorbed water content in the fiber.

2.4. Heat storage model in the nanometer scale

The PCM particle is regarded as a sphere consisting of solid and liquid phases. The heat governing equation of the PCM sphere at location x in the fabric can be modeled by expressing the total heat loss rate from the microspheres in the radial coordinates [38]. The governing equation is given as

$$q_m(x, t) = \begin{cases} \frac{-3\varepsilon_p}{r_m} h_T K_{ml} (T_p - T(x, t)) & T >= T_p, \text{ melting process} \\ h_T r_m \left(\frac{r_m}{r_l(x, t)} - 1 \right) + K_{ml} & \\ \frac{-3\varepsilon_p}{r_m} h_T K_{ms} (T_p - T(x, t)) & T < T_p, \text{ freezing process} \\ h_T r_m \left(\frac{r_m}{r_l(x, t)} - 1 \right) + K_{ms} & \end{cases}, \quad (36)$$

where $q_m(x, t)$ is the energy released/absorbed rate of PCM particle, T_p is the melting point of PCM particle, $T(x, t)$ is the temperature of the flow fields at x , K_{ml} and K_{ms} are the thermal conductivity of liquid and solid PCM particles respectively, h_T is heat transfer coefficient between PCM particles and surrounding flow, ε_p is the volume fraction of PCM, r_m is the radius of micro-PCM spheres, and $r_l(x, t)$ is the radius of the last phase interface in the PCM microcapsules, which is dynamically calculated by:

$$r_l(x, t) = \frac{h_T \frac{K_{ml} r_m^2}{\rho_m \lambda_m} (T_p - T(x, t))}{h_T r_m^2 r_l + (K_{ml} - h_T r_m) r_l^2}. \quad (37)$$

In Eq. (37), λ_m is the latent heat of fusion of PCM particles.

3. Model discretization

In this paper, we consider the implicit finite volume method (FVM) to discretize the PDEs involved in the multiscale models, since FVM has the advantage of unconditional stability, which allows usage of a large time step, and has the flexibility in adapting the time step to control the accuracy of the solution.

Under the FVM, the calculation region is divided into a number of non-overlapping control volumes so that a control volume is present that surrounds each grid point. Hence, we divide the fabric into a number of grids consisting of N control volumes with equal interval size throughout the direction of thickness L .

Let Δx denotes the mesh size ($\Delta x = \frac{L}{N}$) and Δt denotes the time interval, then we can obtain

$$x = \{x_i = i * \Delta x, i = 0, 1, 2, \dots, N\},$$

$$t = \{t_k = k * \Delta t, k = 0, 1, 2, \dots\}.$$

In the discretization region D , we assume the following notations for the space and time functions:

$$C_a(x, t) = C_a(i \Delta x, k \Delta t) = C_a(i, k) = C_{a,i}^k,$$

$$\varepsilon_l(x, t) = \varepsilon_l(i \Delta x, k \Delta t) = \varepsilon_l(i, k) = \varepsilon_{l,i}^k,$$

$$T(x, t) = T(i \Delta x, k \Delta t) = T(i, k) = T_i^k,$$

$$P_s(x, t) = P_s(i \Delta x, k \Delta t) = P_s(i, k) = P_{s,i}^k.$$

Considering the control volume Ω , the PDEs [Eqs. (15)–(18)] can be discretized by approximating their integral values. The integral form of Eq. (15) is re-written as

$$\int_{\Omega} \left[A_1 \frac{\partial C_a}{\partial t} - B_1 \frac{\partial \varepsilon_l}{\partial t} - E_1 - F_1 \right] dx = \int_{\Omega} \left[\frac{\partial}{\partial x} \left(D_1 \frac{\partial C_a}{\partial x} \right) + \frac{\partial}{\partial x} \left(G_a \frac{\partial P_s}{\partial x} \right) \right] dx,$$

where

$$A_1 = \varepsilon_a, \quad B_1 = C_a, \quad E_1 = \sum \varpi_a \varepsilon_f \Gamma_f, \quad F_1 = h_{lg} S_v (C_a^*(T) - C_a),$$

$$D_1 = \frac{\varepsilon_a D_a}{\tau_a}, \quad G_a = C_a \frac{3\varepsilon \sin^2 \alpha d_c^2}{80\mu_a} \left(1 - \left(\frac{\varepsilon_l}{\varepsilon} \right)^3 \right).$$

Its integral value is approximated as

$$\begin{aligned} & A_{1,i}^n \frac{(C_{a,i+1}^{k+1} - C_{a,i}^k)}{\Delta t} \Delta x - B_{1,i}^k \frac{(\varepsilon_{l,i+1}^{k+1} - \varepsilon_{l,i}^k)}{\Delta t} \Delta x - E_{1,i}^k \Delta x - F_{1,i}^k \Delta x \\ &= \left(D_1 \frac{\partial C_a}{\partial x} \right)_{i+\frac{1}{2}} - \left(D_1 \frac{\partial C_a}{\partial x} \right)_{i-\frac{1}{2}} + \left(G_a \frac{\partial P_s}{\partial x} \right)_{i+\frac{1}{2}} - \left(G_a \frac{\partial P_s}{\partial x} \right)_{i-\frac{1}{2}} \\ &= D_{1,i+\frac{1}{2}}^k \frac{(C_{a,i+1}^{k+1} - C_{a,i}^k)}{\Delta x} - D_{1,i-\frac{1}{2}}^k \frac{(C_{a,i}^{k+1} - C_{a,i-1}^k)}{\Delta x} + G_{a,i+\frac{1}{2}}^k \frac{(P_{s,i+1}^{k+1} - P_{s,i}^{k+1})}{\Delta x} - G_{a,i-\frac{1}{2}}^k \frac{(P_{s,i}^{k+1} - P_{s,i-1}^{k+1})}{\Delta x}. \end{aligned}$$

Assuming $\mu = \frac{\Delta t}{\Delta x^2}$, Eq. (15) can be discretized as

$$\begin{aligned} & \left(\mu_{i-\frac{1}{2}} D_{1,i-\frac{1}{2}}^k \right) C_{a,i-1}^{k+1} - \left(A_{1,i}^k + \mu_{i-\frac{1}{2}} D_{1,i-\frac{1}{2}}^k + \mu_{i+\frac{1}{2}} D_{1,i+\frac{1}{2}}^k \right) C_{a,i}^{k+1} + \left(\mu_{i+\frac{1}{2}} D_{1,i+\frac{1}{2}}^k \right) C_{a,i+1}^{k+1} \\ &+ \left(B_{1,i}^k \right) \varepsilon_{l,i}^{k+1} + \left(\mu_{i-\frac{1}{2}} G_{a,i-\frac{1}{2}}^k \right) P_{s,i-1}^{k+1} - \left(\mu_{i-\frac{1}{2}} G_{a,i-\frac{1}{2}}^k + \mu_{i+\frac{1}{2}} G_{a,i+\frac{1}{2}}^k \right) P_{s,i}^{k+1} + \left(\mu_{i+\frac{1}{2}} G_{a,i+\frac{1}{2}}^k \right) P_{s,i+1}^{k+1} \\ &= -A_{1,i}^k C_{a,i}^k + B_{1,i}^k \varepsilon_{l,i}^k - E_{1,i}^k \Delta t - F_{1,i}^k \Delta t. \end{aligned}$$

After summarizing the items, we therefore obtain the final discretized format of Eq. (15) as

$$a_{11,i-1}^k C_{a,i-1}^{k+1} - a_{11,i}^k C_{a,i}^{k+1} + a_{11,i+1}^k C_{a,i+1}^{k+1} + a_{12,i}^k \varepsilon_{l,i}^{k+1} + a_{14,i-1}^k P_{s,i-1}^{k+1} - a_{14,i}^k P_{s,i}^{k+1} + a_{14,i+1}^k P_{s,i+1}^{k+1} = R_{1,i}^k, \quad (38)$$

where

$$\begin{aligned} a_{11,i-1}^k &= \mu_{i-\frac{1}{2}} D_{1,i-\frac{1}{2}}^k, & a_{11,i}^k &= A_{1,i}^k + \mu_{i-\frac{1}{2}} D_{1,i-\frac{1}{2}}^k + \mu_{i+\frac{1}{2}} D_{1,i+\frac{1}{2}}^k, & a_{11,i+1}^k &= \mu_{i+\frac{1}{2}} D_{1,i+\frac{1}{2}}^k, & a_{12,i}^k &= B_{1,i}^k, \\ a_{14,i-1}^k &= \mu_{i-\frac{1}{2}} G_{a,i-\frac{1}{2}}^k, & a_{14,i}^k &= \mu_{i-\frac{1}{2}} G_{a,i-\frac{1}{2}}^k + \mu_{i+\frac{1}{2}} G_{a,i+\frac{1}{2}}^k, & a_{14,i+1}^k &= \mu_{i+\frac{1}{2}} G_{a,i+\frac{1}{2}}^k, \\ R_{1,i}^k &= -A_{1,i}^k C_{a,i}^k + B_{1,i}^k \varepsilon_{l,i}^k - F_{1,i}^k \Delta t - F_{1,i}^k \Delta t. \end{aligned}$$

The integral form of Eq. (16) is re-written as

$$\int_{\Omega} \left[A_2 \frac{\partial \varepsilon_l}{\partial t} + E_2 - F_2 \right] dx = \int_{\Omega} \left[\frac{\partial}{\partial x} \left[D_2 \frac{\partial \varepsilon_l}{\partial x} \right] + \frac{\partial}{\partial x} \left[G_l \frac{\partial P_s}{\partial x} \right] \right] dx,$$

where,

$$A_2 = \rho_l, \quad E_2 = \sum \varpi_l \varepsilon_f \Gamma_f, \quad F_2 = h_{lg} S_v (C_a^*(T) - C_a),$$

$$D_2 = \frac{\rho_l D_l}{\tau_l}, \quad G_l = \rho_l \frac{3\varepsilon \sin^2 \beta d_c^2}{80\mu_l} \left(\frac{\varepsilon_l}{\varepsilon} \right)^3.$$

Similarly, the final discretized form of Eq. (16) is

$$a_{22,i-1}^k \varepsilon_{l,i-1}^{k+1} - a_{22,i}^k \varepsilon_{l,i}^{k+1} + a_{22,i+1}^k \varepsilon_{l,i+1}^{k+1} + a_{24,i-1}^k P_{s,i-1}^{k+1} - a_{24,i}^k P_{s,i}^{k+1} + a_{24,i+1}^k P_{s,i+1}^{k+1} = R_{2,i}^k, \quad (39)$$

where

$$\begin{aligned} a_{22,i-1}^k &= \mu_{i-\frac{1}{2}} (D_2)_{i-\frac{1}{2}}^k, & a_{22,i}^k &= A_{2,i}^k + \mu_{i-\frac{1}{2}} (D_2)_{i-\frac{1}{2}}^k + \mu_{i+\frac{1}{2}} (D_2)_{i+\frac{1}{2}}^k, & a_{22,i+1}^k &= \mu_{i+\frac{1}{2}} (D_2)_{i+\frac{1}{2}}^k, \\ a_{24,i-1}^k &= \mu_{i-\frac{1}{2}} (G_2)_{i-\frac{1}{2}}^k, & a_{24,i}^k &= \mu_{i-\frac{1}{2}} (G_l)_{i-\frac{1}{2}}^k + \mu_{i+\frac{1}{2}} (G_l)_{i+\frac{1}{2}}^k, & a_{24,i+1}^k &= \mu_{i+\frac{1}{2}} (G_l)_{i+\frac{1}{2}}^k, \\ R_{2,i}^k &= -A_{2,i}^k \varepsilon_{l,i}^k + E_{2,i}^k \Delta t - F_{2,i}^k \Delta t. \end{aligned}$$

The integral form of Eq. (17) is re-written as

$$\int_{\Omega} \left[A_3 \frac{\partial T}{\partial t} - C_3 - E_3 + F_3 - G_3 - H_3 \right] dx = \int_{\Omega} \left[\frac{\partial}{\partial x} \left[D_3 \frac{\partial T}{\partial x} \right] \right] dx,$$

where

$$A_3 = c_v, \quad C_3 = \frac{\partial F_R}{\partial x} - \frac{\partial F_L}{\partial x}, \quad E_3 = \sum (\varpi_a \lambda_v + \varpi_l \lambda_l) \varepsilon_f \Gamma_f, \quad F_3 = \lambda h_{lg} S_v (C_a^*(T) - C_a).$$

$$G_3 = q_m, \quad H_3 = W, \quad E_3 = K.$$

The final discretized form of Eq. (17) is

$$a_{33,i-1}^k T_{i-1}^{k+1} - a_{33,i}^k T_i^{k+1} + a_{33,i+1}^k T_{i+1}^{k+1} = R_{3,i}^k, \quad (40)$$

where

$$\begin{aligned} a_{33,i-1}^k &= \mu_{i-\frac{1}{2}} D_{3,i-\frac{1}{2}}^k, & a_{33,i}^k &= A_{3,i}^k + \mu_{i-\frac{1}{2}} D_{3,i-\frac{1}{2}}^k + \mu_{i+\frac{1}{2}} D_{3,i+\frac{1}{2}}^k, & a_{33,i+1}^k &= \mu_{i+\frac{1}{2}} D_{3,i+\frac{1}{2}}^k, \\ R_{3,i}^k &= -A_{3,i}^k T_i^k - C_{3,i}^k \Delta t - E_{3,i}^k \Delta t + F_{3,i}^k \Delta t - G_{3,i}^k \Delta t - H_{3,i}^k \Delta t. \end{aligned}$$

The integral form of Eq. (18) is re-written as

$$\int_{\Omega} \left[A_4 \frac{\partial P_s}{\partial t} + B_4 \frac{\partial T}{\partial t} + C_4 \frac{\partial \varepsilon_l}{\partial t} + E_4 - F_4 \right] dx = \int_{\Omega} \left[\frac{\partial}{\partial x} \left[G_s \frac{\partial P_s}{\partial x} \right] \right] dx,$$

where,

$$\begin{aligned} A_4 &= \frac{M_g \varepsilon_a}{RT}, & B_4 &= P_s \frac{\varepsilon_a M_g}{RT^2}, & C_4 &= \frac{M_g P_s}{RT}, & E_4 &= \varpi_a \varepsilon_f \frac{\partial C_f}{\partial t} \\ F_4 &= h_{lg} S_v (C_a^*(T) - C_a), & G_s &= \frac{M_s P_s}{RT} \frac{3\varepsilon \sin^2 \alpha d_c^2}{80\mu_a} \left(1 - \left(\frac{\varepsilon_l}{\varepsilon} \right)^3 \right). \end{aligned}$$

The final discretized form of Eq. (18) is

$$a_{43,i}^k T_i^{k+1} - a_{42,i}^k \varepsilon_{l,i}^{k+1} + a_{44,i-1}^k P_{s,i-1}^{k+1} - a_{44,i}^k P_{s,i}^{k+1} + a_{44,i+1}^k P_{s,i+1}^{k+1} = R_{4,i}^k, \quad (41)$$

where

$$\begin{aligned} a_{43,i}^k &= -B_{4,i}^k, \quad a_{42,i}^k = C_{4,i}^k, \quad a_{44,i-1}^k = \mu_{i-\frac{1}{2}}(G_s)_{i-\frac{1}{2}}^k, \quad a_{44,i}^k = A_{4,i}^k + \left(\mu_{i-\frac{1}{2}}(G_s)_{i-\frac{1}{2}}^k \right) + \left(\mu_{i+\frac{1}{2}}(G_s)_{i+\frac{1}{2}}^k \right), \\ a_{44,i+1}^k &= \mu_{i+\frac{1}{2}}(G_s)_{i+\frac{1}{2}}^k \\ R_{4,i}^k &= -A_{4,i}^k P_{s,i}^k - B_{4,i}^k T_i^k - C_{4,i}^k \varepsilon_{l,i}^k + E_{4,i}^k \Delta t - F_{4,i}^k \Delta t. \end{aligned}$$

Similarly, the final discretized form of Eq. (34) on the fiber radius direction is:

$$\left(\mu \eta r_{i-\frac{1}{2}} D_{f,i-\frac{1}{2}}^n \right) C_{f,i-1}^{k+1} - \left(\mu \eta r_{i+\frac{1}{2}} D_{f,i+\frac{1}{2}}^n + \mu \eta r_{i-\frac{1}{2}} D_{f,i-\frac{1}{2}}^n + 1 \right) C_{f,i}^{k+1} + \left(\mu \eta r_{i+\frac{1}{2}} D_{f,i+\frac{1}{2}}^n \right) C_{f,i+1}^{k+1} = -C_{f,i}^k, \quad (42)$$

where

$$\mu = \frac{\Delta t}{\Delta r^2}, \quad \eta = \frac{2}{r_{i-\frac{1}{2}} + r_{i+\frac{1}{2}}}.$$

4. Numerical solutions

In the discretized equations, $C_{a,i}^{k+1}$, $\varepsilon_{l,i}^{k+1}$, T_i^{k+1} and $P_{s,i}^{k+1}$ denote the water vapor concentration in the inter-fiber void space, the volume proportion of the liquid moisture, and the temperature and pressure of air in the porous fabric, respectively, at time $(k+1)\Delta t$ and at grid position $i\Delta x$. Because Eqs. (15)–(18) are coupled, the discrete Eqs. (38)–(41) can form the linear algebraic equations as:

$$A_h X^h = B_h, \quad (43)$$

where

$$X^h = [C_{a,0}^{k+1}, C_{a,1}^{k+1}, \dots, C_{a,n}^{k+1}, \varepsilon_{l,0}^{k+1}, \varepsilon_{l,1}^{k+1}, \dots, \varepsilon_{l,n}^{k+1}, T_0^{k+1}, T_1^{k+1}, \dots, T_n^{k+1}, P_{s,0}^{k+1}, P_{s,1}^{k+1}, \dots, P_{s,n}^{k+1}]^T,$$

$$B^h = [R_{1,0}^k, R_{1,1}^k, \dots, R_{1,n}^k, R_{2,0}^k, R_{2,1}^k, \dots, R_{2,n}^k, R_{3,0}^k, R_{3,1}^k, \dots, R_{3,n}^k, R_{4,0}^k, R_{4,1}^k, \dots, R_{4,n}^k]^T$$

$$A_h = \begin{bmatrix} a_{11,0}^k & a_{11,1}^k & \cdots & 0 & 0 & 0 & \cdots & 0 & 0 & 0 & \cdots & 0 & 0 & 0 & \cdots & 0 \\ a_{11,0}^k & a_{11,1}^k & a_{11,2}^k & \cdots & 0 & 0 & a_{12,2}^k & 0 & 0 & 0 & \cdots & 0 & 0 & a_{14,1}^k & a_{14,2}^k & \cdots \\ 0 & \cdots & \cdots & 0 & 0 & 0 & 0 & \cdots & 0 & 0 & \cdots & 0 & 0 & 0 & \cdots & \cdots \\ 0 & a_{11,n-2}^k & a_{11,n-1}^k & a_{11,n}^k & 0 & 0 & a_{12,n-2}^k & 0 & 0 & 0 & \cdots & 0 & 0 & a_{14,n-1}^k & a_{14,n}^k & \cdots \\ 0 & 0 & \cdots & 0 & a_{22,0}^k & a_{22,1}^k & \cdots & 0 & 0 & 0 & \cdots & 0 & 0 & 0 & \cdots & 0 \\ 0 & 0 & \cdots & 0 & a_{22,0}^k & a_{22,1}^k & a_{22,2}^k & 0 & 0 & 0 & \cdots & 0 & 0 & a_{24,1}^k & a_{24,2}^k & 0 \\ 0 & 0 & \cdots & 0 & 0 & 0 & \cdots & 0 & 0 & 0 & \cdots & 0 & 0 & 0 & \cdots & \cdots \\ 0 & 0 & \cdots & 0 & 0 & a_{22,n-2}^k & a_{22,n-1}^k & a_{22,n}^k & 0 & 0 & \cdots & 0 & 0 & a_{24,n-1}^k & a_{24,n}^k & \cdots \\ 0 & 0 & \cdots & 0 & 0 & 0 & \cdots & 0 & a_{33,0}^k & a_{33,1}^k & \cdots & 0 & 0 & 0 & \cdots & 0 \\ 0 & 0 & \cdots & 0 & 0 & 0 & 0 & a_{33,0}^k & a_{33,1}^k & a_{33,2}^k & \cdots & 0 & 0 & 0 & \cdots & 0 \\ 0 & 0 & \cdots & 0 & 0 & 0 & 0 & 0 & 0 & 0 & \cdots & 0 & 0 & 0 & \cdots & 0 \\ 0 & 0 & \cdots & 0 & 0 & 0 & 0 & 0 & 0 & a_{33,n-2}^k & a_{33,n-1}^k & a_{33,n}^k & 0 & 0 & \cdots & 0 \\ 0 & 0 & \cdots & 0 & 0 & 0 & 0 & 0 & 0 & 0 & 0 & \cdots & 0 & a_{44,0}^k & a_{44,1}^k & 0 & 0 \\ 0 & 0 & \cdots & 0 & 0 & 0 & a_{42,2}^k & \cdots & 0 & 0 & a_{43,2}^k & \cdots & a_{44,0}^k & a_{44,1}^k & a_{44,2}^k & 0 \\ 0 & 0 & \cdots & 0 & 0 & 0 & \cdots & \cdots & 0 & \cdots & \cdots & 0 & 0 & 0 & \cdots & \cdots \\ 0 & 0 & \cdots & 0 & 0 & 0 & a_{43,n-2}^k & 0 & 0 & 0 & a_{43,n-2}^k & 0 & a_{44,n-2}^k & a_{44,n-1}^k & a_{44,n}^k \end{bmatrix}.$$

Since A_h is not strictly diagonally dominant, X^h can be easily solved by Gaussian elimination, in which the upper triangular matrix from A_h is obtained by performing a sequence of elementary row operations. Since all the unknown items ($C_{a,i}^{k+1}$, $\varepsilon_{l,i}^{k+1}$, T_i^{k+1} and $P_{s,i}^{k+1}$) cannot be solved point by point through the known items ($C_{a,i}^k$, $\varepsilon_{l,i}^k$, T_i^k and $P_{s,i}^k$), they are solved by these simultaneous linear algebraic equations, which lead to the advantage that this algorithm is unconditional stable [39].

Thus, the numerical scheme for the thermal smart clothing system simulation can be implemented following the scales of different sub-systems, as shown in Fig. 2. The detail steps are listed in Table 1.

5. Model validation and application

5.1. Model validation

In order to validate the simulation capacity of proposed multiscale models, the predicted results were compared to the experimental results of a set of smart clothing reported in previous publications [40, 41] with the same clothing materials and experimental conditions.

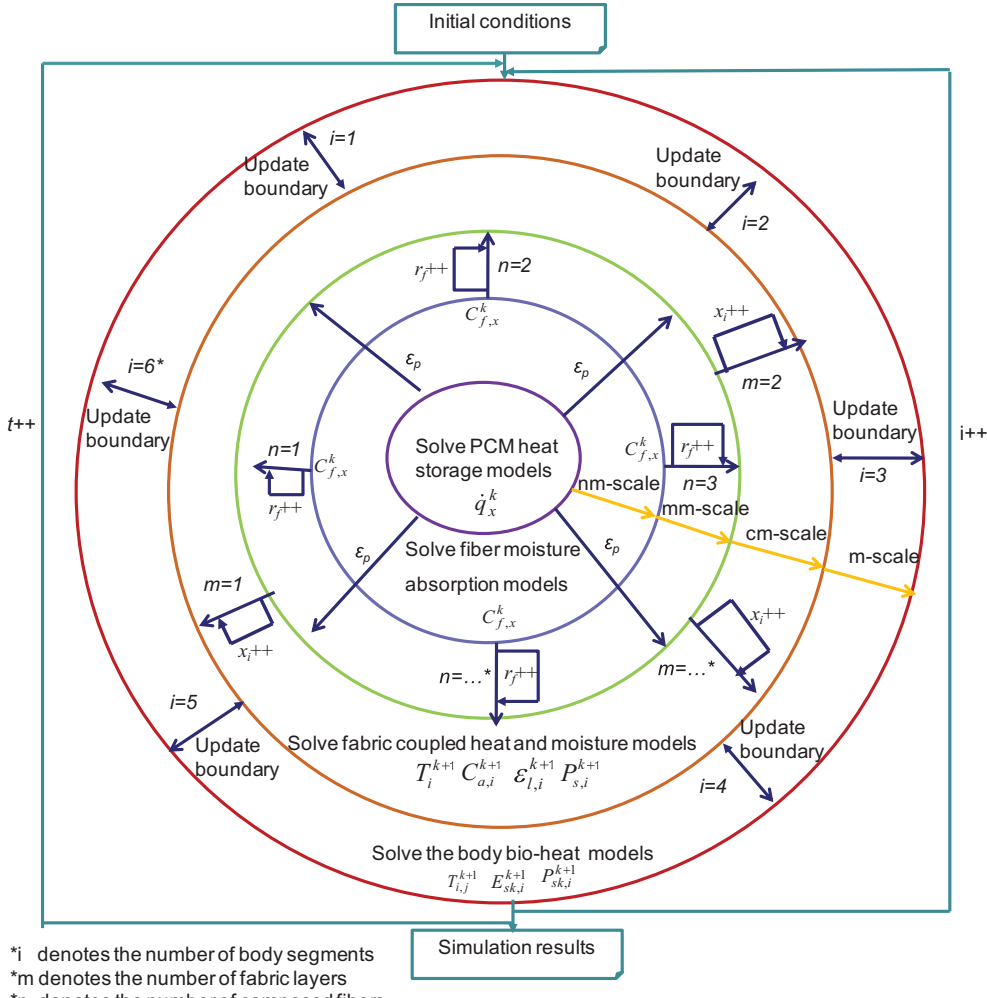


Fig. 2. Numerical scheme of thermal smart clothing system simulation.

Table 1

Detail steps in the numerical scheme.

Step 1: Initializing the human body, the clothing that covers the individual body parts and the simulation scenarios in terms of the garment style (p_m , p_h), body activity (M), and activity duration (t). We assume the initial physiological variables of the body ($T_0, M_0, B_0, K_0, D_0, E_0, P_{sk,0}$) by referring to the standard state of the body [24]. The clothing on the individual body parts is initialized with the initial state of the body (C_{sk}, T_{sk}) and the initial environment (C_e, T_e, P_{s0}) as:

$$\begin{cases} C_a(x, 0) = (C_{sk}, C_e) \\ T(x, 0) = (T_{sk}, T_e); \\ \varepsilon_l(x, 0) = S_0 \\ P_s(x, 0) = P_{s0} \\ C_f(x, 0) = f(T, RH); \end{cases} \quad (44)$$

Step 2: Providing the simulation control information: (1) the grid number of the fabric mesh along the fabric thickness (x); (2) the grid number of fiber mesh along the fiber radius (r_f); (3) the time step (t) for the interval of simulation iteration.

Step 3: Solving the PCM heat storage model in Eqs. (36) and obtaining the value of q_x^k in the nm-scale.

Step 4: Solving the fiber moisture absorption/desorption model in Eqs. (34) with the grid number of fiber mesh (r_f^{++}) and obtaining the value of $C_{f,x}^k$ on the fiber mesh in the mm-scale, then repeating the solution for all the fibers composed for the fabric.

Step 5: Calculating the coefficients $a_{i,j}^k$ and $R_{i,j}^k$ in Eqs. (38)–(41) to construct the matrix A_h in Eq. (43), solving the fabric coupled heat and moisture transfer models in Eqs. (15)–(18) with the grid number of fabric mesh (x^{++}) and obtain the value of $C_{a,i}^{k+1}, \varepsilon_{l,i}^{k+1}, T_i^{k+1}$ and $P_{s,i}^{k+1}$ on the fabric mesh in the cm-scale, then repeating the solution for all the fabrics in the smart clothing.

Step 6: Solving the human body bio-heat transfer model in Eqs. (1)–(2) by finite difference approximation and obtaining the solution of $T_{i,j}^{k+1}, E_{sk,i}^{k+1}, P_{sk,i}^{k+1}$ on the individual body part in the m-scale, and then updating the boundary conditions in Eqs.(24)–(31) for all fabric coupled heat and moisture transfer models responding to each body segment.

Step 7: Iterating steps 2–6 according to the time interval (Δt) until all the activity duration in the simulation ends.

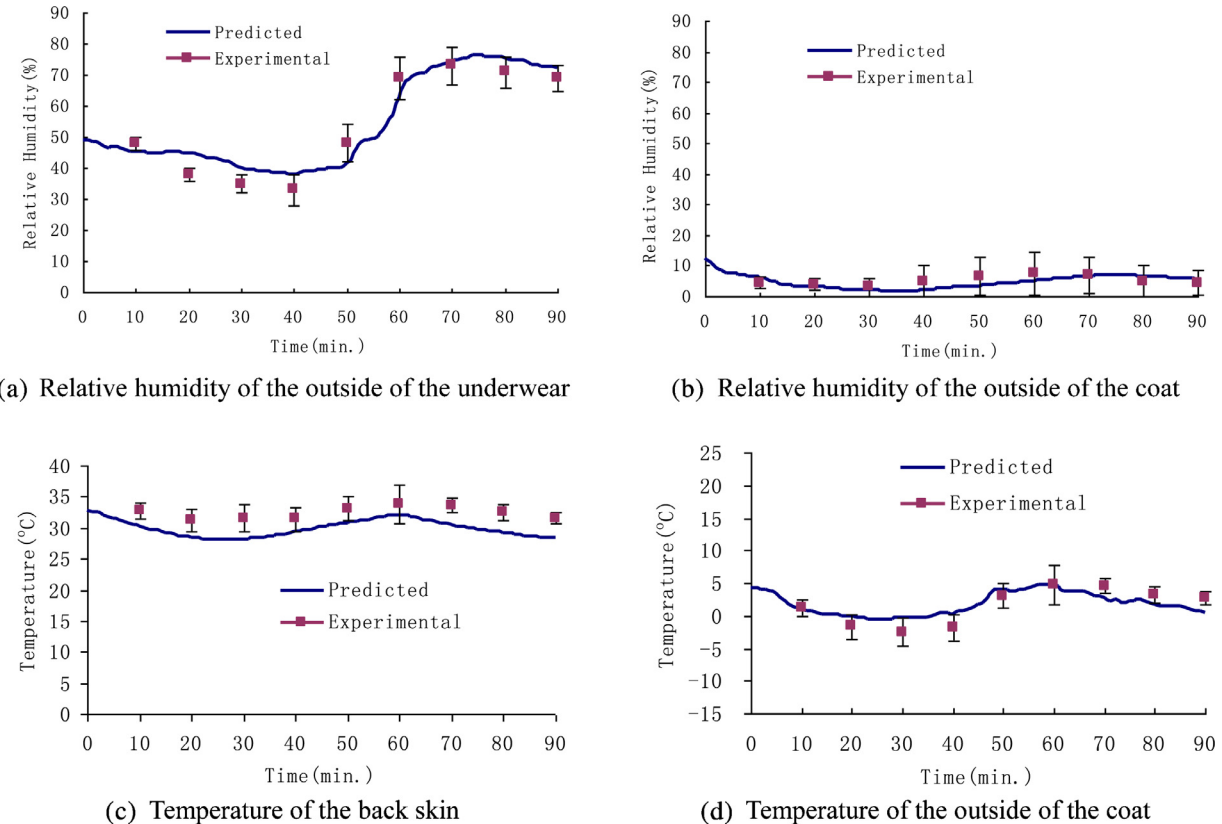


Fig. 3. Comparison between the predicted and experimental results of the clothing treated by moisture management.

In reference [40], the smart clothing consists of underwear (wool–cotton), vest (nylon–polyester), coat (nylon–polyester) and outer jacket (nylon–polyester), in which all the inner fabric layers in the clothing were treated by moisture management function. The wearing scenarios were specified as the human body in a cold environment of -15°C temperature, 30% relative humidity and 0.1 m/s^2 wind velocity. A group of subjects wearing the clothing performed sitting resting (30 mins), running at a velocity of 6.4 km/h (30 mins) and sitting resting again (30 mins). Thermal sensors were attached on the body skin and clothing to measure the temperature and relative humidity.

The predicted results by the multiscale models under the same wearing scenarios were compared with the measured data in the experiment in terms of relative humidity of the outside of the underwear, relative humidity of the outside of the coat, temperature of the back skin and temperature of the outside of the coat, as shown in Fig. 3. It is seen that the predicted and experimental results distributions throughout the wearing scenario have good agreement. The predicted values almost are in the standard deviation of the experimental values.

Meanwhile, the calculation simulation was performed according to the reference [41], in which the set of smart clothing was coated with PCM (phase change material) and have the same wearing protocols. Similarly, the comparisons were made between the predicted and experimental results of the temperature of the back skin and the temperature of the outside of the coat, which can be easy to observe the effect of PCM on the heat distributions. As shown in Fig. 4, the predicted values are almost within the range of the error bars of the experimental ones, indicating a good agreement between them.

5.2. Application

A design case of a set of thermal smart clothing with PCM coating and self-heating wires is presented in this section. Basically, the clothing is long style and constructed with a fabric layer, which is weaved by mixing cotton and wool fibers. To provide better functions, it may be treated with PCM particles and self-heating wires. In practical design, in order to develop a good functional design scheme, designers need to confirm the following design issues including: (1) the different thermal biological response of all body parts when wearing the clothing; (2) the different thermal distributions of the clothing on all body parts; (3) the different thermal performance of all fiber materials in the fabric; (4) the different thermal performance of the clothing when being treated with different volume of PCM and different heating power of self-heating wires.

Based on the multi-scale models and numerical solution, the thermal smart clothing may be numerically designed and simulated in specified wearing scenarios to help the designers to confirm these issues. In this design case, the human wearing this

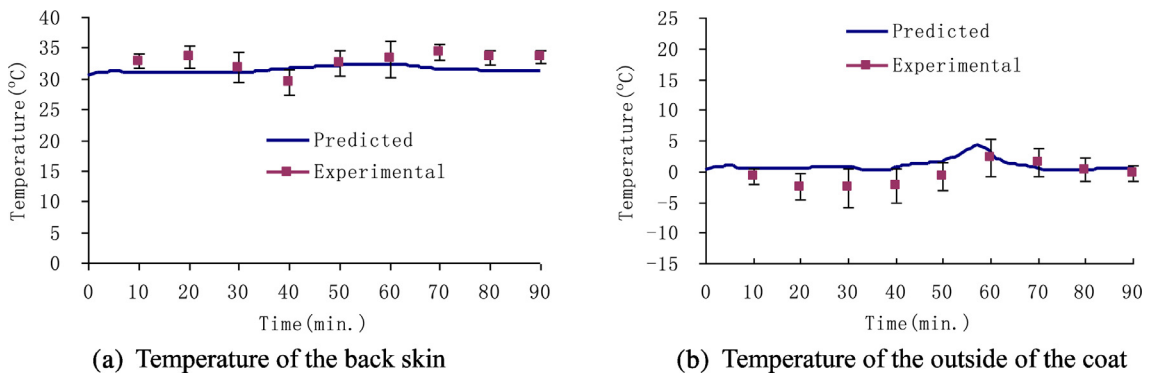


Fig. 4. Comparison between the predicted and experimental results of clothing coated with PCM.

Table 2
Thermal properties of the fabric used in the thermal smart clothing.

Physical properties	Value	Unit
Fiber radius (r_f)	0.1	mm
Weight (W_f)	223	g/m ²
Thickness (L)	1.26	cm
Thermal conductivity (K_f)	0.065	W/m/K
Water vapor permeability (WVP)	885	g/24h/cm ²
Porosity (ε)	0.75	
PCM volume proportion (ε_p)	0.1	
Heating rate of self-heating wires (W)	2.5	cal/s/cm ³
Bottom temperature of self-heating wires (T_b)	22	°C
Top temperature of self-heating wires (T_h),	25	°C

Table 3
Thermal properties of PCM used for the fabric.

Physical properties	Value	Unit
Microsphere radius (r_m)	0.01	mm
Melting point (T_p)	28	°C
Latent fusion heat (λ_m)	238.7	KJ/Kg
Density at 20 °C (ρ_m)	779	Kg/m ³
Thermal conductivity of liquid PCM (K_{ml})	0.3	W/m/K
Thermal conductivity of solid PCM (K_{ms})	0.4	W/m/K
Heat transfer coefficient between PCM microcapsules and surrounding flow fields (h_T)	0.01195	W/m ² .K

Table 4
Important thermal parameters used in the simulation.

Parameters	Value	Unit
Convective heat transfer coefficient H_c	0.17	W/m ² .K
Convective mass transfer coefficient H_m	810	m/s
Heat of sorption of water vapor λ_v	$2522.0 + 1602.5e^{-11.72}$	kJ/kg
Heat of sorption of liquid water λ_l	$1602.5e^{-11.72}$	kJ/kg
Mass transfer coefficient for evaporation/ condensation h_{lg}	0.17	m/s
Radiative absorption constant of the fiber β	74.27	m/s
Dynamic viscosity of liquid water η	1.0×10^{-3}	Kg/m.s
Proportion of water vapor transferred from the clothed skin p_m	0.9	
Proportion of heat loss at the clothed skin p_h	0.9	

clothing is specified as a standard male person with 80 kg weight and 1.8 m² body surface area [22]. The wearing environment is with air temperature $T_e = 20$ °C, air relative humidity $RH = 65\%$ and air pressure $P_{s0} = 1.0135e5$ Pa. The wearing scenarios included 30-min resting, 30-min walking at 5 km/h and 30-min sitting. The thermal properties of the fabric and PCM used in the simulation are listed in Tables 2 and 3 respectively, and the values of the important parameters used in the simulation are listed in Table 4.

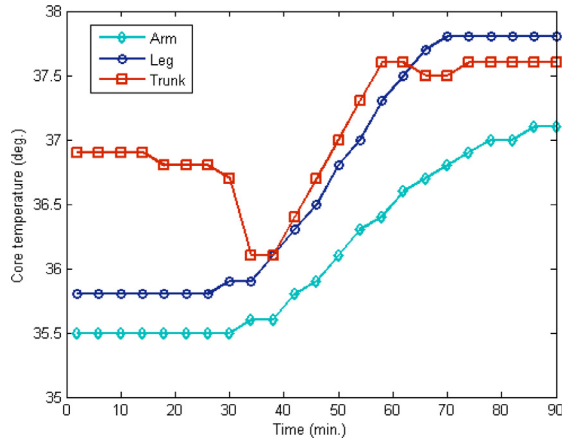


Fig. 5. Core temperature distribution.

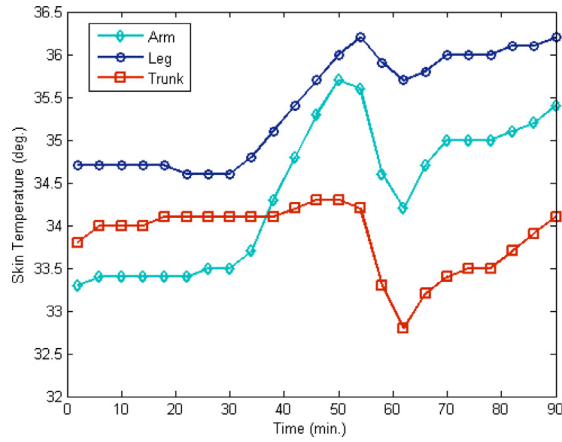


Fig. 6. Skin temperature distribution.

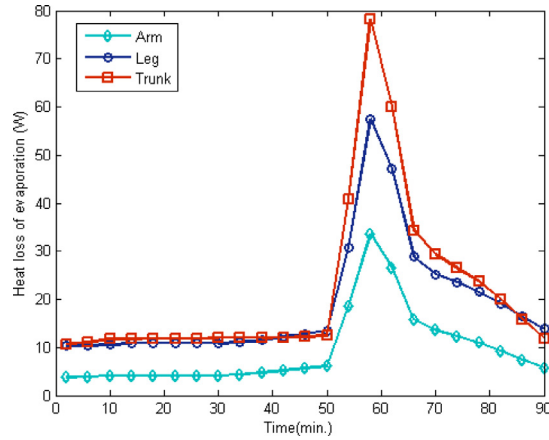


Fig. 7. Heat loss due to evaporation from the skin.

Through the simulation results distribution and comparison, the designers are helpful to obtain a direct confirmation on the above issues. They are discussed as follows:

Figs. 5–8 show the biological temperature distribution in the human body, including the skin temperature, core temperature, heat loss due to evaporation from the skin, and pressure on the skin of the arm, leg, and trunk during the simulation. Fig. 5 shows that the core temperature in the body increased during the sitting–walking–resting stages. In overall, the core temperature of the different body parts arises during the exercise. However, there is a sudden drop of the core temperature of the trunk when

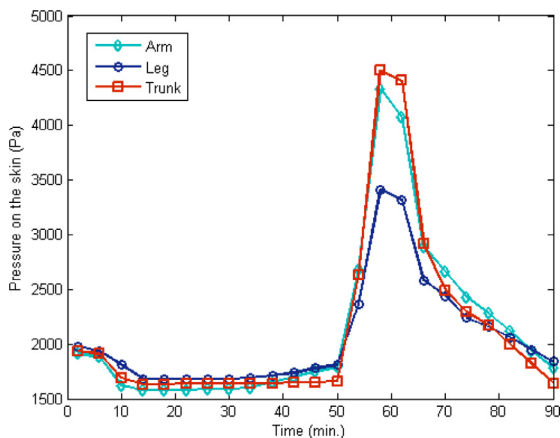


Fig. 8. Pressure on the skin.

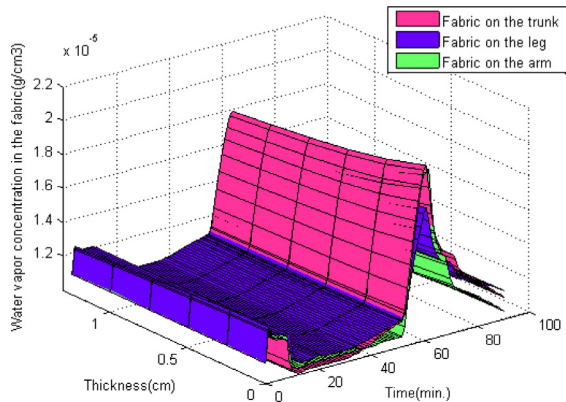
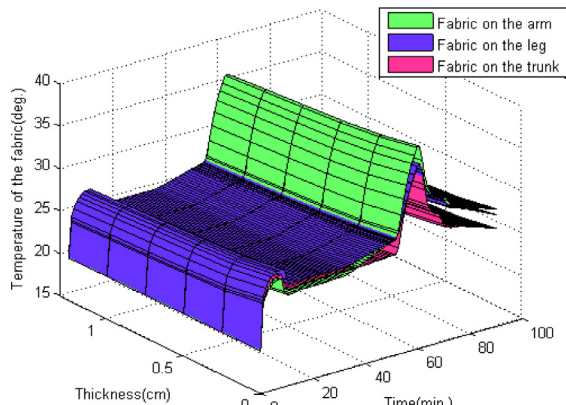


Fig. 9. Water vapor concentration distribution on the fabrics.



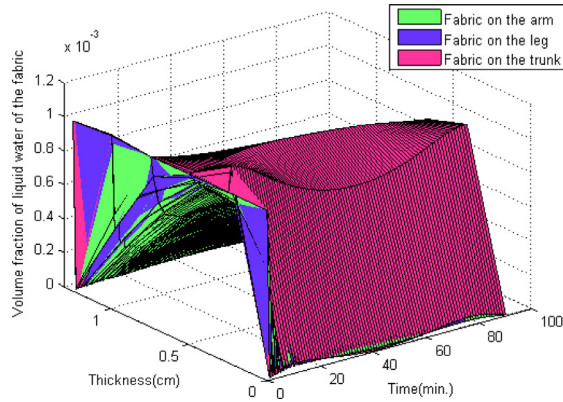


Fig. 11. Volume fraction of the liquid water distribution on the fabrics.

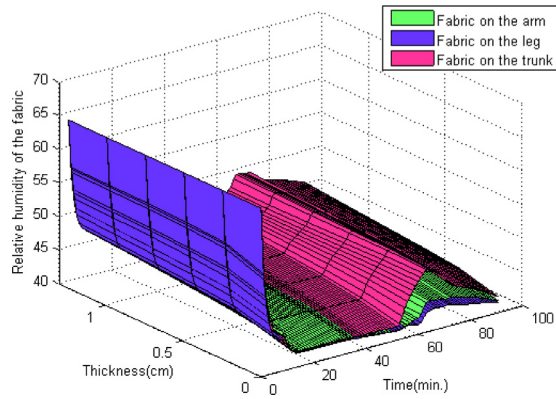


Fig. 12. Relative humidity distribution on the fabrics.

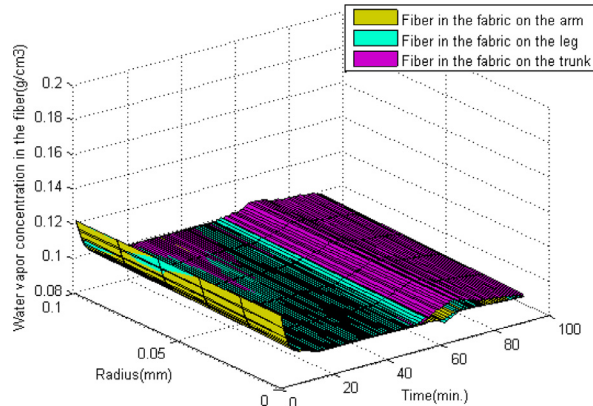


Fig. 13. Water vapor concentration distribution of the cotton fiber on the fabrics.

loss due to sweat evaporation during the walking stage was caused by the airflow encountered on the body during walking, which was also reflected by the pressure on the skin, as shown in Fig. 8. The trunk and leg, with more sweat volume and more direct exposure to the airflow, exhibited a greater heat loss because of the evaporation on the skin and, thus, had the lowest increase in skin temperature during the walking stage.

We simulated the coupled heat and moisture transfer process in the textile material of the garment that cover the body parts corresponding to the trunk, arm, and leg. Figs. 9–12 show the thermal distribution of the fabrics on the arm, leg, and trunk, including the water vapor concentration, temperature, volume fraction of liquid water, and relative humidity.

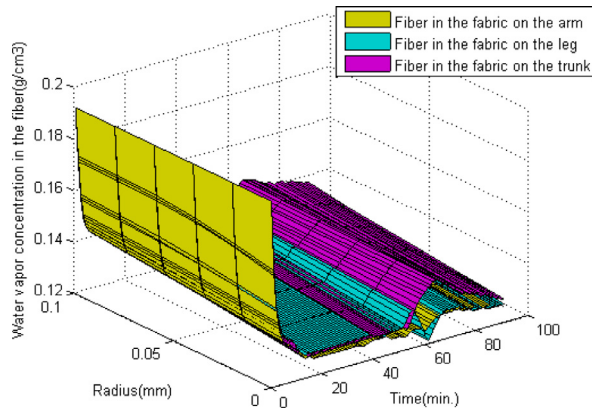


Fig. 14. Water vapor concentration distribution of the wool fiber on the fabrics.

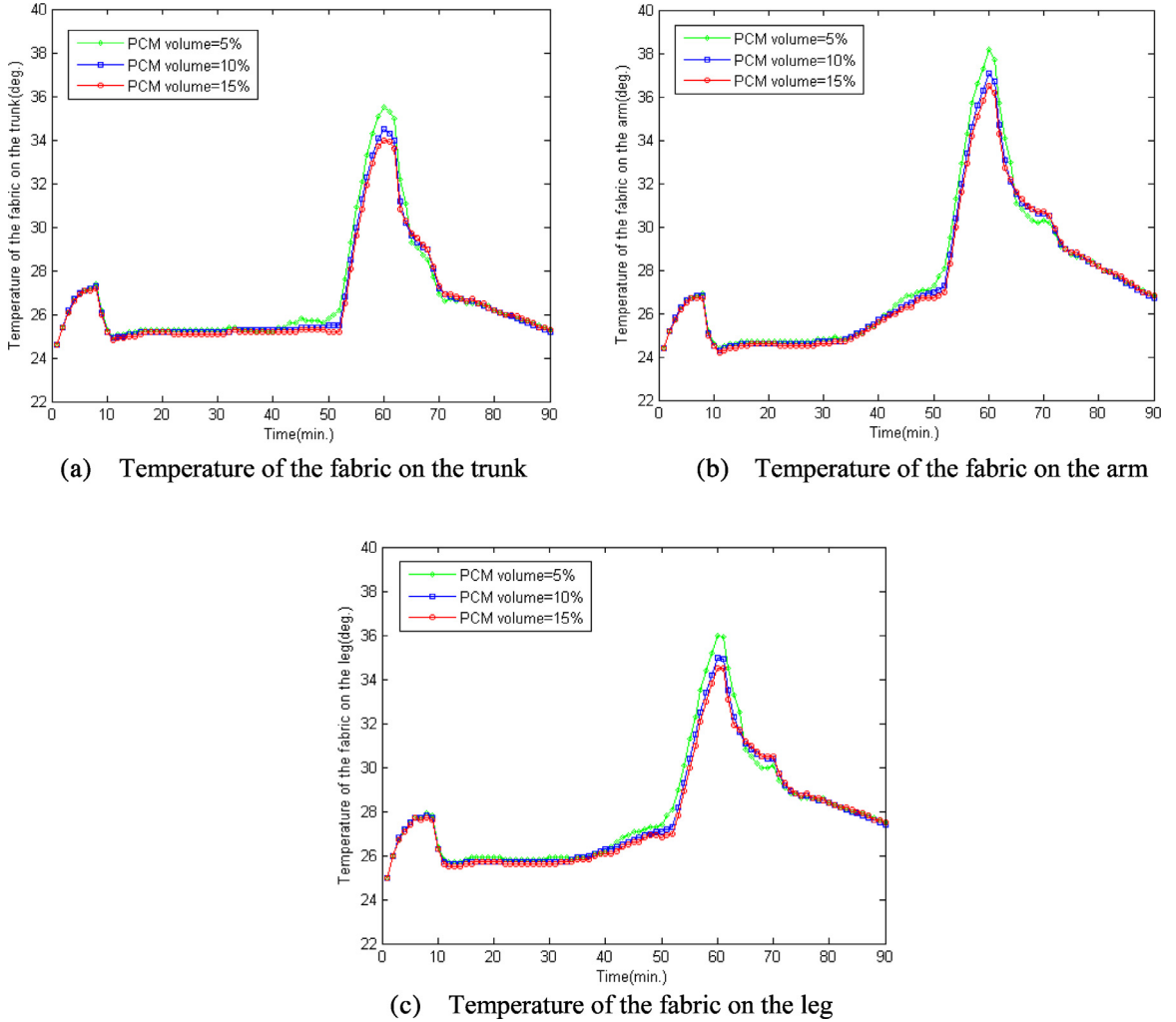


Fig. 15. Temperature distributions of the fabric on different body parts under different PCM volumes.

[Fig. 9](#) shows that the water vapor concentration on the fabrics became stable during the resting stage and increased when the human body sweated during the walking stage. It finally fell down again when the body stopped walking and entered the sitting stage. The vapor moisture was transferred from the inner side ($L \rightarrow 1.26$ cm) to the outer side ($L \rightarrow 0$ cm) of the fabrics because of the moisture diffusion across the fabric. From the comparison of the results shown in [Fig. 9](#), the water vapor concentration

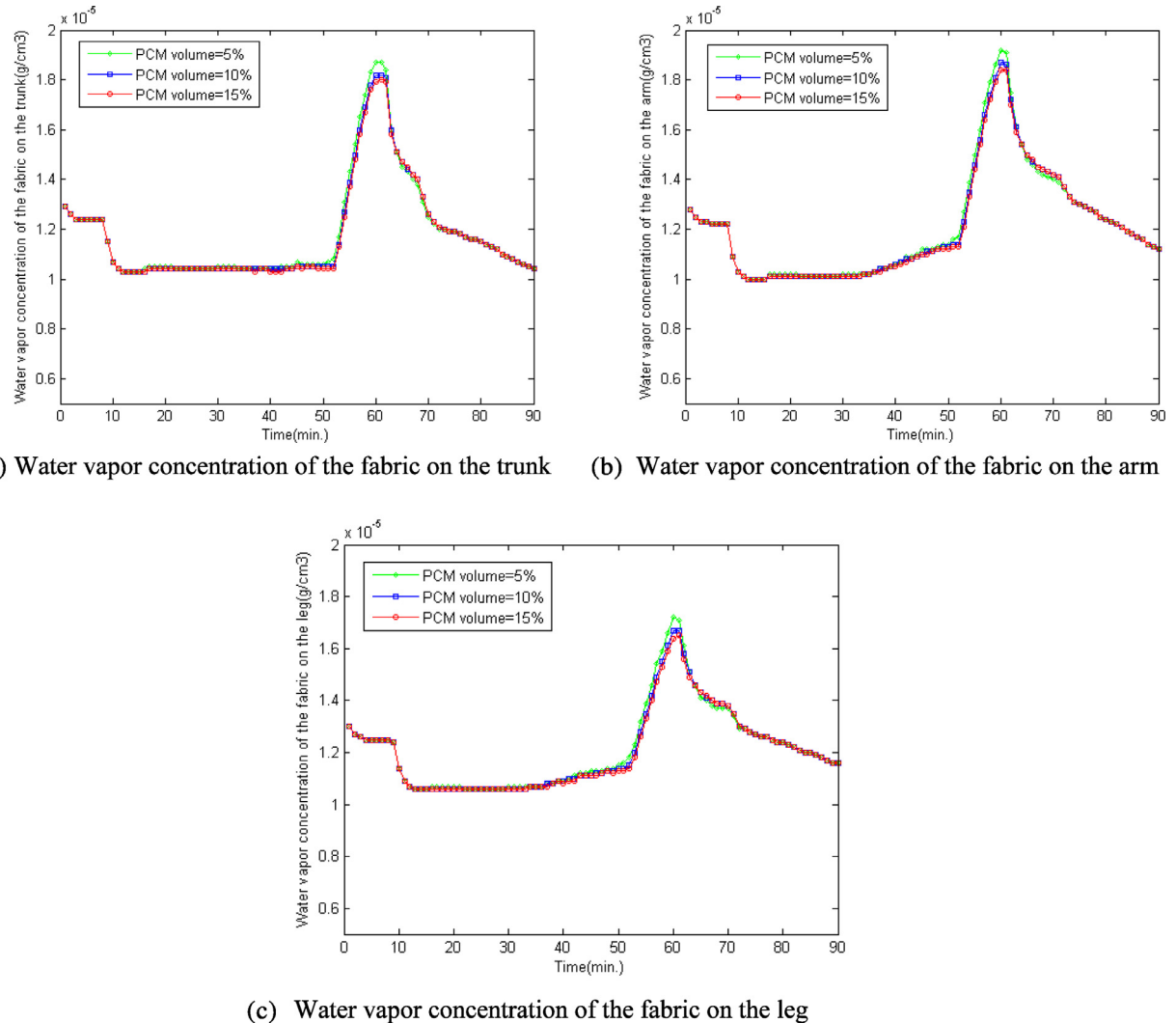


Fig. 16. Water vapor concentration distributions of the fabric on different body parts under different PCM volumes.

on the fabrics on the trunk greatly increased compared with those of the legs and arms because of the highest amount of sweat generated. The lower moisture concentration on the fabric on the leg is due to the fewer sweat glands in the lower limbs of the body.

Similarly, Fig. 10 shows the temperature distribution on the fabrics, which started to increase after some time during the walking stage and decreased during the sitting stage. However, the temperature of the fabric on the trunk exhibited the lowest increase because of the largest heat loss due to sweating. Meantime, the temperature of the fabric on the arm increase to be the highest due to the least sweating and evaporation heat loss on the arm. This fact agreed with the results shown in Figs. 6 and 7. The lower skin temperature and the greater heat loss due to sweating in the trunk influence the temperature distribution on the fabrics on the trunk and leg through the interaction between the skin and the fabric.

A trend was established that showed that the trunk underwent much sweating, as shown in Figs. 11 and 12, indicating that the fabric on the trunk had greater volume fraction of liquid water and relative humidity than those of the other body parts. Through capillary effect on the interstices in the fibers, liquid water was transferred across the fabrics in the direction of the thickness.

Figs. 13–14 show the water vapor concentration distribution of the cotton and wool fibers on the fabrics on the trunk, arm, and leg. The cotton and wool fibers on the trunk have higher water vapor concentration than those of the other parts because the fabric on the trunk has more vapor moisture. Figs. 13–14 show that the wool fiber has higher water vapor concentration than the cotton fiber, which agrees with the fact that wool has better moisture absorption ability than cotton.

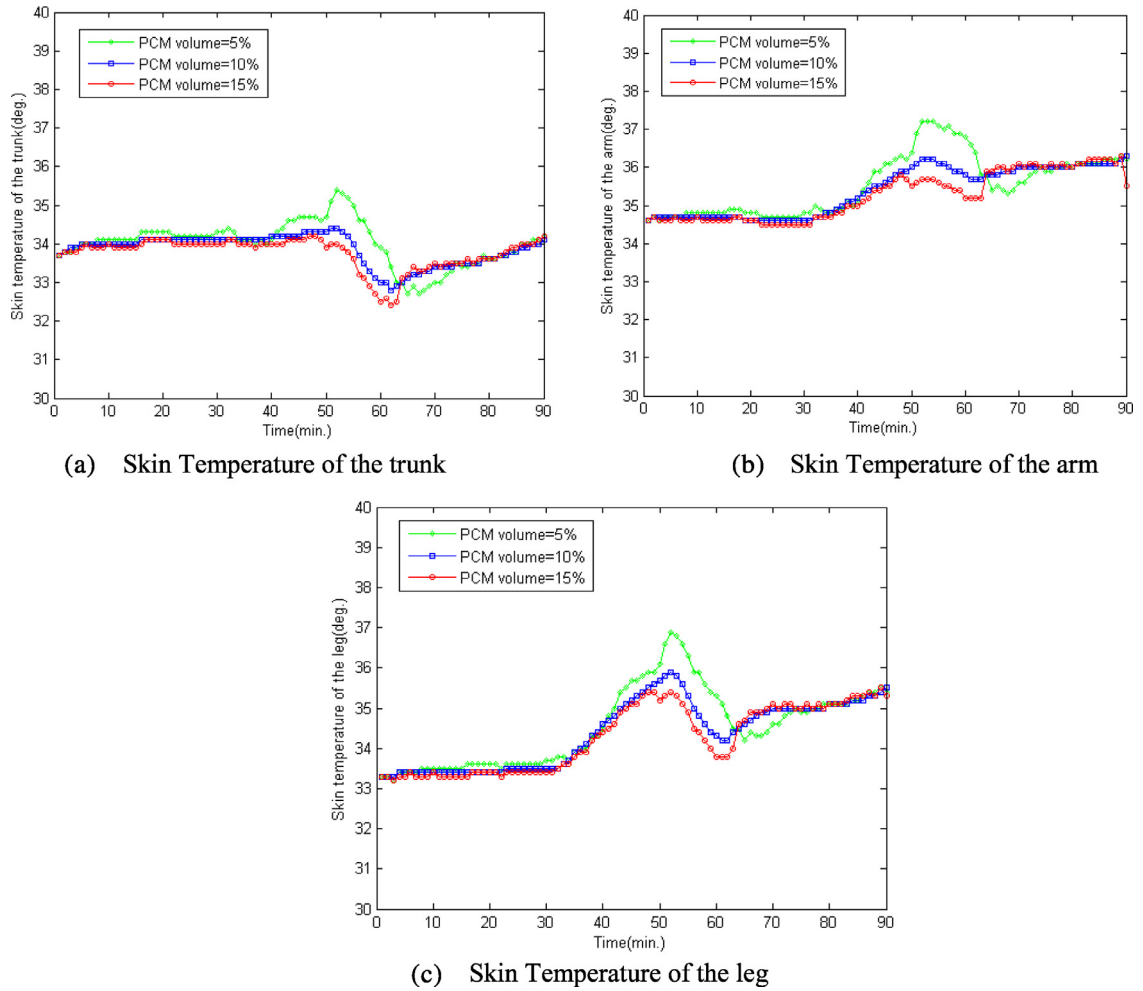


Fig. 17. Skin temperature distributions of different body parts under different PCM volumes.

The role of the PCM particles incorporated into the fabric is to influence the temperature of the fabric owing to the heat released/absorbed by the PCM particles. In order to investigate how the PCM influence the thermal functions of different parts of the clothing and see the different body parts responses, we simulated the smart clothing with different PCM volumes in the same wearing scenarios, and compared the temperature and water vapor concentration distributions of the middle point of the fabric ($L = 0.63$ cm) as well as the skin temperature on the different body parts, as shown in Figs. 15–17. Through these distribution charts, it can be seen that the larger the PCM volume of the fabric is treated, the greater delaying effect of transient change of temperature and water vapor concentration of the fabric has, and thus the slower change of the skin temperature is obtained. It can also be seen that the more volume of PCM coating have greater influence on the thermal distributions of the fabric and the skin temperature during the sudden thermal change, and this phenomenon is more obvious on the parts of arm and leg which have higher temperature than the trunk from the walking stage.

Meanwhile, in order to investigate the effect of different heating rates of self-heating wires on the thermal performance of the clothing and human body, we simulated the smart clothing with the same wearing protocol while under different heating rates. The temperature of the middle point of the fabric ($L = 0.63$ cm) in these cases are compared in Fig. 18, which shows the higher heating rate leads to greater increase of the fabric's temperature. Fig. 19 depicts the skin temperature of different body parts response to the fabric with different heating rates. It can also be seen that the skin temperature of the arm has less decrease during the walking stage due to the higher fabric temperature, which may be caused by the less sweating evaporation heat.

From the above discussion, we can see that the involved complex thermal processes and properties of the thermal smart clothing wearing system can be numerically predicted having good agreement with the experimental results. Through numerical simulation, the different thermal biological response of different body parts when wearing the clothing, the different thermal distributions of the clothing on individual body parts and even the different thermal performance of all fiber materials in the fabric can be predicted during the whole simulation scenarios, which illustrate the thermal performance of clothing during wearing; Furthermore, the different thermal performance of the clothing when being treated with different volume of PCM or

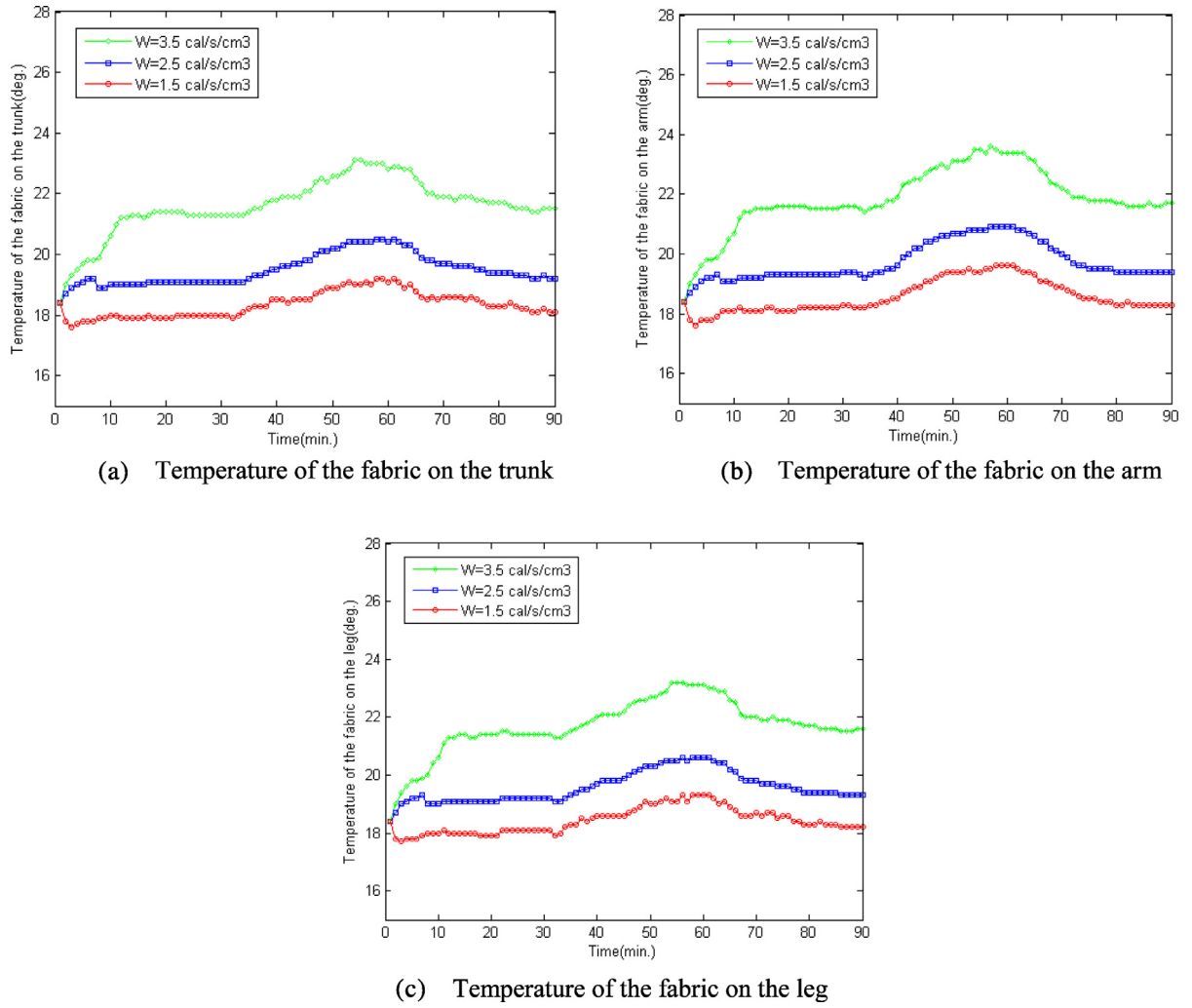


Fig. 18. Temperature distributions of the fabric on different body parts under different self-heating rates.

different heating rates of self-heating wires can be predicted and compared to see their influence on the thermal functions of the clothing. The proposed design issues in the design can be investigated and thus have a detailed analysis by the simulation results presentation. These predictions and analysis are beneficial to the designers to try different thermal smart designs of the clothing and confirm the thermal quality of different design before they make real samples, which may greatly reduce the design cost [42,43].

6. Conclusion

This paper has presented a numerical algorithm to simulate the thermal smart clothing system using a group of multi-scale nonlinear models. Mathematical models have been proposed to describe the mix-type multi-scale heat and moisture behaviors in the human body on the meter scale, the fabric on the millimeter scale, the fiber materials on the micrometer scale, and the PCM particles on the nanometer scale. Furthermore, the thermal functional treatments on the clothing, such as moisture management treatment, waterproof membrane and self-heating technology are considered in the models. These different scale models were integrated by describing their interactions through the boundary. The FVM was adopted to discretize the coupled nonlinear PDEs in this group of models. Based on the model discretization, the numerical scheme was developed with a clear computational procedure following the scales of all sub-systems. The simulation models have been validated by comparing the predicted results with the experimental results in references, showing good agreement between them. A series of simulation in a design case of thermal smart clothing was presented to show that it can preview and analyze the thermal and moisture distributions in the body, fabric, and fiber, as well as the influence of the PCM particles and the self-heating treatment in the design through the numerical simulation, thus the expected design issues can be investigated and the optimal design scheme can be figured out. The simulation capability by this numerical algorithm is helpful for the designers in the engineering design

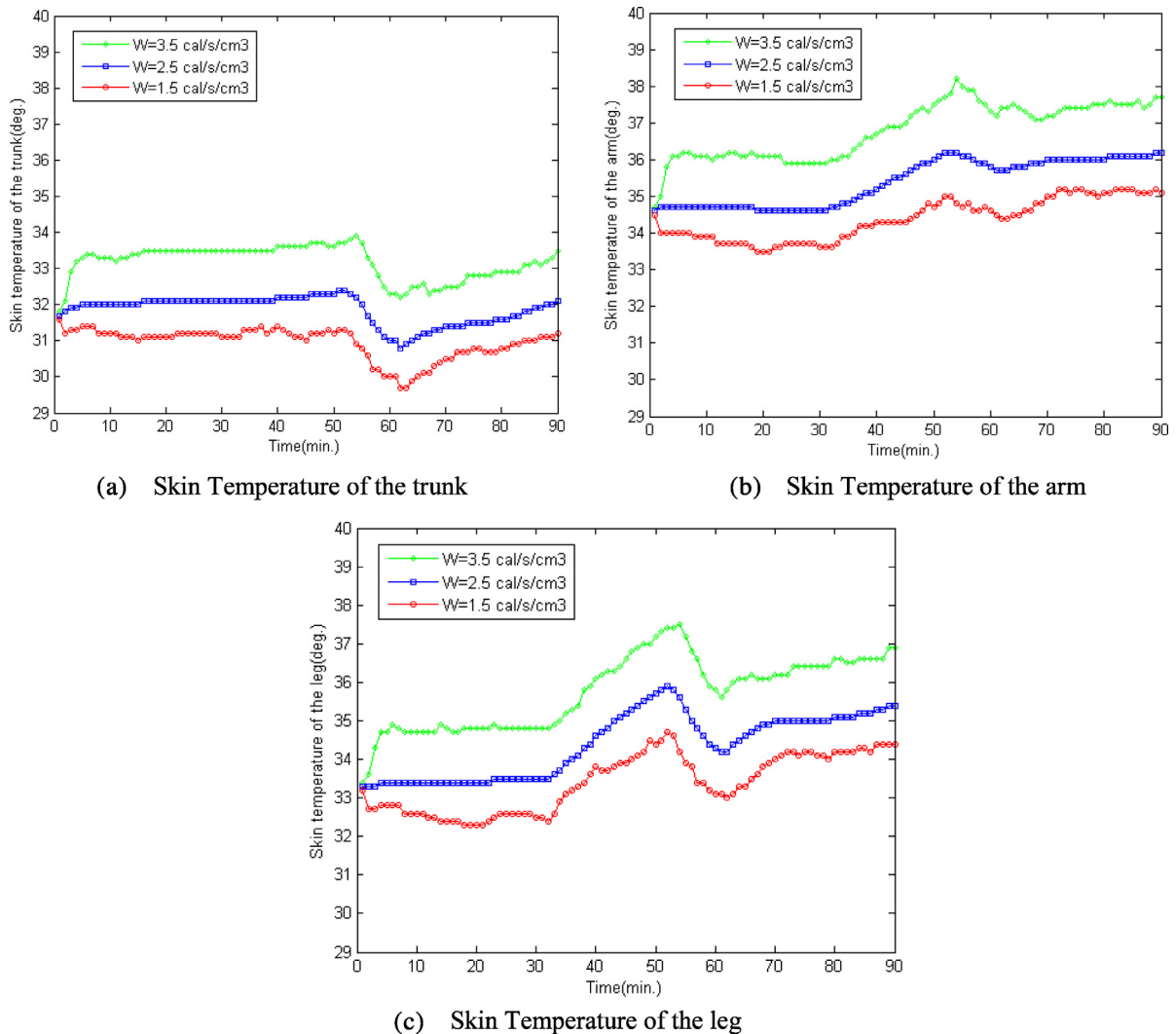


Fig. 19. Skin temperature distributions of different body parts under different self-heating rates.

process to early identify the thermal quality of clothing, determine the design scheme without making real prototypes and thus reduce the design cost.

Acknowledgments

The work of this paper is financially supported by the National Natural Science Foundation of China (No. 61502112), the Science and Technology Planning Project of Guangdong Province (No. 2015A030401030, 2015A020219014, 2013B021600011), the Science and Technology Planning Project of Guangzhou City (No. 2014J4100158) and the MOE (Ministry of Education in China) Project of Humanities and Social Sciences (No.13YJC890027), the Guangdong Province Universities and Colleges Excellent Youth Teacher Training Program .

References

- [1] B. Farnworth, Mechanisms of heat flow through clothing insulation, *Textile Res. J.* 53 (1983) 717–725.
- [2] S.A. Whitaker, Simultaneous heat, mass and moment transfer in porous media, in: J.P. Hartnett (Ed.), *A Theory of Drying in Porous Media*, in: *Advances in Heat Transfer*, Academic Press, New York, 1977, pp. 119–200.
- [3] C.H. Shen, G.S. Springer, Moisture absorption and desorption of composite materials, *J. Compos. Mater.* 10 (1) (1976) 2–20.
- [4] J. Bear, *Dynamics of Fluids in Porous Media*, Elsevier, New York, 1972.
- [5] I.C. Watt, Kinetic studies of the wool-water system, Part I: the mechanisms of two-stage absorption, *Textile Res. J.* 30 (1960) 644–651.
- [6] Y. Li, B.V. Holcombe, A two-stage sorption model of the coupled diffusion of moisture and heat in wool fabric, *Textile Res. J.* 62 (1992) 211–217.
- [7] P. Nordon, H.G. David, Coupled diffusion of moisture and heat in hygroscopic textile materials, *Textile Res. J.* 37 (10) (1967) 853–866.
- [8] P.S.H. Henry, Diffusion in absorbing media, *Proc. R. Soc. London. Series A*, 171 (1939) 215–241.

- [9] J.T. Fan, X.H. Wen, Modeling heat and moisture transfer through fibrous insulation with phase change and mobile condensates, *Int. J. Heat Mass Transfer* 45 (2002) 4045–4055.
- [10] C.V. Le, N.G. Ly, R. Postle, Heat and mass transfer in the condensing flow of steam through an absorbing fibrous medium, *Int. J. Heat Mass Transfer* 38 (1995) 81–89.
- [11] Q.Y. Zhu, Y. Li, Effects of pore size distribution and fiber diameter on the coupled heat and liquid moisture transfer in porous textiles, *Int. J. Heat Mass Transfer* 46 (2003) 5099–5111.
- [12] Z. Wang, Y. Li, Q.Y. Zhu, Z.X. Luo, Radiation and conduction heat transfer coupled with liquid water transfer, moisture sorption and condensation in porous polymer materials, *J. Appl. Polym. Sci.* 89 (2003) 2780–2790.
- [13] K. Min, Y. Son, C. Kim, Y. Lee, H. Hong, Heat and moisture transfer from skin to environment through fabrics: a mathematical model, *Int. J. Heat Mass Transfer* 50 (2007) 5292–5304.
- [14] Y.S. Chen, J. Fan, W. Zhang, Clothing thermal insulation during sweating, *Textile Res. J.* 73 (2003) 152–157.
- [15] X.F. Wan, J.T. Fan, A transient thermal model of the human body–clothing–environment system, *J. Therm. Biol.* 33 (2008) 87–97.
- [16] K. Ghali, N. Ghaddar, B. Jones, Modeling of heat and moisture transport by periodic ventilation of thin cotton fibrous media, *Int. J. Heat Mass Transfer* 45 (2002) 3703–3714.
- [17] G. Fu, A Transient, 3-D Mathematical Thermal Model for the Clothed Human, Kansas State University, : Kansas, 1995, p. 270.
- [18] S.I. Green, Z. Wang, T. Waung, A. Vakil, Simulation of the flow through woven fabrics, *Comput. Fluids* 37 (9) (2008) 1148–1156.
- [19] C. Ye, H. Huang, J. Fan, W. Sun, Numerical study of heat and moisture transfer in textile materials by a finite volume method, *Commun. Comput. Phys.* 4 (2008) 929–948.
- [20] H.H. Pennes, Analysis of tissue and arterial blood temperature in the resting human forearm, *J. Appl. Physiol.* 1 (1948) 93–122.
- [21] S. Weinbaum, L. Jiji, Theory and experiment for the effect of vascular temperature on surface tissue heat transfer – part 1: anatomical foundation and model conceptualization, *ASME J. Biomed. Eng.* 106 (1984) 246–251.
- [22] A.P. Gagge, J.A.J. Stolwijk, Y. Nishi, An effective temperature scale based on a simple model of human physiological regulatory response, *ASHRAE Trans.* 77 (1971) 247–262.
- [23] J.A.J. Stolwijk, J.D. Hardy, Control of body temperature, in: R.G. Stephen (Ed.), *Handbook of Physiology-Reaction to Environmental Agents*, Wiley-Blackwell, 1977, pp. 45–67.
- [24] N. Ghaddar, K. Ghali, B. Jones, Integrated human-clothing system model for estimating the effect of walking on clothing insulation, *Int. J. Therm. Sci.* 42 (2003) 605–619.
- [25] N. Ghaddar, K. Ghali, S. Chehaitly, Assessing thermal comfort of active people in transitional spaces in presence of air movement, *Energy Build.* 43 (10) (2011) 2832–2842.
- [26] Y.D. Cheng, J.L. Niu, N.P. Gao, Thermal comfort models: a review and numerical investigation, *Build. Environ.* 47 (2012) 13–22.
- [27] M. Salloum, N. Ghaddar, K. Ghali, A new transient bioheat model of the human body and its integration to clothing models, *Int. J. Therm. Sci.* 46 (2007) 371–384.
- [28] S. Tanabe, K. Kobayashi, J. Nakano, Y. Ozeki, M. Konishi, Evaluation of thermal comfort using combined multi-node thermoregulation (65MN) and radiation models and computational fluid dynamics(CFD), *Energy Build.* 34 (2002) 637–646.
- [29] C. Huizinga, Z. Hui, A model of human physiology and comfort for assessing complex thermal environments, *Build. Environ.* 36 (2001) 691–699.
- [30] D. Fiala, K.J. Lomas, M. Stohrer, Computer predictions of human thermoregulatory and temperature responses to a wide range of environment conditions, *Int. J. Biometeorol.* 45 (2001) 143–159.
- [31] S.C. Tanabe, K. Kobayashi, J. Nakano, Y. Ozeki, Evaluation of thermal comfort using combined multi-node thermoregulation (65MN) and radiation models and computational fluid dynamics (CFD), *Energy Build.* 34 (2002) 637–646.
- [32] B.W. Jones, Y. Ogawa, Transient interaction between the human and the thermal environment, *ASHRAE Trans.* (1992) 98 Part 1().
- [33] Y. Li, Q.Y. Zhu, Simultaneous heat and moisture transfer with moisture sorption, condensation and capillary liquid diffusion in porous textiles, *Textile Res. J.* 73 (6) (2003) 515–524.
- [34] F.Z. Li, Y. Li, Y.X. Liu, Z.X. Luo, Numerical simulation of coupled heat and mass transfer in hygroscopic porous materials considering the influence of atmospheric pressure, *Numer. Heat Transfer Part B* (45) (2004) 249–262.
- [35] Y. Li, Z.X. Luo, An improved mathematical simulation of the coupled diffusion of moisture and heat in wool fabric, *Textile Res. J.* 69 (10) (1999) 760–768.
- [36] A.H. Mao, Y. Li, Numerical heat transfer coupled with multi-dimensional liquid moisture diffusion in porous textiles with a measurable-parameterized model, *Numer. Heat Transfer, Part A Appl.* 56 (2009) 1–23.
- [37] Z. Wang, Y. Li, C.Y. Yeung, Y.L. Kwok, Influence of waterproof fabrics on coupled heat and moisture transfer in a clothing system, *J. Soc. Fiber Sci. Technol.* 59 (5) (2003) 187–195.
- [38] Y. Li, Q.Y. Zhu, A model of heat and moisture transfer in porous textiles with phase change materials, *Textile Res. J.* 74 (5) (2004) 447–457.
- [39] W.X. Zhong, X.L. Zhuang, J.P. Zhu, A self-adaptive time integration algorithm for solving partial differential equations, *Appl. Math. Comput.* 89 (1998) 295–312.
- [40] S.X. Wang, Y. Li, H. Tokura, J.Y. Hu, Y.X. Han, Y.L. Kwok, R.W. Au, Effect of moisture management on functional performance of cold protective clothing, *Textile Res. J.* 77 (12) (2008) 968–980.
- [41] S.X. Wang, Y. Li, H. Tokura, J.Y. Hu, Y.L. Kwok, R.W. Au, Effect of phase change materials on temperature and moisture distributions in clothing during exercise in cold environment, in: The 1st Textile Bioengineering and Informatics Symposium, Hong Kong, 2008.
- [42] A.H. Mao, Y. Li, X.N. Luo, R.M. Wang, S.X. Wang, A CAD system for multi-style thermal functional design of clothing, *Comput.-Aided Des.* 40 (2008) 916–930.
- [43] A.H. Mao, J. Luo, Y. Li, X.N. Luo, R.M. Wang, A multi-disciplinary strategy for computer-aided clothing thermal engineering design, *Comput.-Aided Des.* 43 (12) (2011) 1854–1869.